

# Hyperchaos in the generalized Rössler system

Th. Meyer, M.J. Bünner, A. Kittel, J. Parisi

*Faculty of Physics, Department of Energy and Semiconductor Research, University of Oldenburg, D-26111 Oldenburg, Germany*

(March 21, 2022)

Introduced as a model for hyperchaos, the generalized Rössler system of dimension  $N$  is obtained by linearly coupling  $N - 3$  additional degrees of freedom to the original Rössler equation. Under variation of a single control parameter, it is able to exhibit the chaotic hierarchy ranging from fixed points via limit cycles and tori to chaotic and, finally, hyperchaotic attractors. By the help of a mode transformation, we reveal a structural symmetry of the generalized Rössler system. The latter will allow us to interpret number, shape, and location in phase space of the observed coexisting attractors within a common scheme for arbitrary odd dimension  $N$ . The appearance of hyperchaos is explained in terms of interacting coexisting attractors. In a second part, we investigate the Lyapunov spectra and related properties of the generalized Rössler system as a function of the dimension  $N$ . We find scaling properties which are not similar to those found in homogeneous, spatially extended systems, indicating that the high-dimensional chaotic dynamics of the generalized Rössler system fundamentally differs from spatio-temporal chaos. If the time scale is chosen properly, though, a universal scaling function of the Lyapunov exponents is found, which is related to the real part of the eigenvalues of an unstable fixed point.

PACS number: 05.45.+b

## I. INTRODUCTION

Chaotic dynamics has been intensively investigated with the help of simple low-dimensional models like the Lorenz [1] or the Rössler system [2]. Because of the restricted phase space, only low-dimensional chaotic motion is observed in these systems. Low-dimensional chaos can also be observed in nature [3], although the underlying dynamical systems have an infinite number of degrees of freedom. One may wonder: What is the connection of this low-dimensional chaos to the truly high-dimensional states, that may arise out of chaos under variation of one control parameter? How does the transition from the low-dimensional to the high-dimensional states take place?

Consider the attractors of dissipative ordinary differential equations under variation of the dimension  $N$  of phase space. Rössler [4] has postulated a chaotic hierarchy where more and more qualitatively new forms of complex motion develop with increasing dimension: In one dimension, only stable fixed points are encountered. In two dimensions, also periodic orbits can exist. In three dimensions, the possibility of quasiperiodicity and chaos arises. Thus, at the lower end of the hierarchy, the well-known low-dimensional dynamical states of motion can be found. Somewhere high up in the hierarchy, things like turbulence or noise may be located. One crucial question is, how one can distinguish and characterize the higher steps of the hierarchy. A provisional classification can be made in terms of Lyapunov exponents [5]. For dynamical states with more than one positive Lyapunov exponent, the term hyperchaos has been coined [6]. In order to study the full chaotic hierarchy, Baier and Sahle [7] have introduced a class of model equations, the *Generalized Rössler System* (furtheron called GRS). Starting from the Rössler system as one of the simplest and best understood nonlinear ordinary differential equations that exhibit chaos, the GRS is obtained by linearly coupling additional degrees of freedom to the original Rössler system. The structure of the GRS of dimension  $N$  is that of an  $N - 1$  dimensional linear subsystem that is coupled to one nonlinear variable. As will be shown, the GRS preserves essential characteristics of the Rössler system while extending it to a phase space of arbitrary dimension  $N$ . This allows to study the influence of the discrete parameter  $N$ , without having to compare completely different systems.

Baier and Sahle [7] demonstrated that the GRS does, indeed, show hyperchaotic dynamics with an increasing number of positive Lyapunov exponents for increasing  $N$ . The GRS realizes one possible path through the complete chaotic hierarchy from a stable fixed point via periodic orbits and chaos up to hyperchaos. We [8] have introduced a mode transformation of the GRS based on the numerical solution of the linear subsystem. In the present paper, we will restate the mode transformation based on a semianalytical solution of the linear subsystem. The mode transformation will then be used to analyze the dynamics of the GRS with arbitrary dimension  $N$  in phase space. In Section II, the GRS is introduced and general properties of the GRS are discussed. In Section III, we deal with the mode transformation and the concept of structural symmetry, that later on will allow us to understand the number, the form, and the location of the coexisting attractors of the GRS. Subsequently, we numerically investigate the dynamics of the GRS in phase space for the cases  $N = 5$  and  $N = 7$  in Section IV. We interpret the observed dynamics within a

general scheme that enables to predict the structure of the attractors for higher  $N$ . In Section V, then, we investigate the GRS in the hyperchaotic state for different values of the dimension  $N$ . We report scaling properties of the number of positive Lyapunov exponents, the Lyapunov dimension, the metric entropy, and the Lyapunov spectra as a function of  $N$ . The limit  $N \rightarrow \infty$  is discussed in view of the literature on that subject.

## II. GENERAL PROPERTIES OF THE GENERALIZED RÖSSLER SYSTEM

The GRS is given by

$$\frac{d}{dt}\mathbf{x}(t) = A\mathbf{x}(t) - x_N(t)\mathbf{e}_{N-1} \quad (1)$$

$$\frac{d}{dt}x_N(t) = \varepsilon + bx_N(t)(x_{N-1}(t) - d) , \quad (2)$$

where

$$A = \begin{pmatrix} a & -1 & 0 & \dots & 0 \\ 1 & 0 & -1 & \ddots & \vdots \\ 0 & 1 & \ddots & -1 & 0 \\ \vdots & \ddots & 1 & 0 & -1 \\ 0 & \dots & 0 & 1 & 0 \end{pmatrix}, \quad \mathbf{x}(t) = \begin{pmatrix} x_1(t) \\ \vdots \\ x_{N-1}(t) \end{pmatrix} ,$$

$$\mathbf{e}_{N-1} = \begin{pmatrix} 0 \\ \vdots \\ 0 \\ 1 \end{pmatrix}, \quad \mathbf{x}(t), \mathbf{e}_{N-1} \in \mathcal{R}^{N-\infty} .$$

It is composed of an  $N-1$  dimensional linear subsystem  $\mathbf{x}$  and one nonlinear variable  $x_N$ . Qualitatively, the mechanism of instability of the GRS is the same as that of the Rössler system for all dimensions  $N$ . The positive feedback or autocatalytic process that is controlled by the parameter  $a$  causes an expansive dynamics of the GRS around the origin. As long as  $x_{N-1}$  remains well below the threshold  $d$  of  $x_N$ ,  $x_N$  adiabatically follows its equilibrium value  $\varepsilon/b(d - x_{N-1})$  and does not influence the linear subsystem  $\mathbf{x}$  appreciably. When  $x_{N-1}$  comes close to or exceeds  $d$ ,  $x_N$  will start to grow rapidly, thereby folding the system back to a state of lower amplitude (via  $\mathbf{e}_{N-1}$  in Eq. (1)). This time development of  $x_N$  of long intervals of small amplitude interrupted by short spikes leads us to call  $x_N$  the *nonlinear trigger*.

One of the three parameters  $\varepsilon$ ,  $b$ , and  $d$  can be eliminated by rescaling the amplitude of  $(\mathbf{x}, x_N)$ . In the form the equations are given in (1), (2), they are scaled in time in such a way that the (angular) eigenfrequencies of the linear subsystem lie in the interval  $[0, 2]$  for all values of  $N$  (see Section III).

The divergence of the GRS is  $a + b(x_{N-1} - d)$ , independent of  $N$ . Thus, the GRS is dissipative, if  $\langle x_{N-1} \rangle < d - \frac{a}{b}$  (the angle brackets denote the time average). This is true for all parameter values to be considered in the following.

For odd  $N$ , the linear subsystem  $\mathbf{x}$  can be transformed into  $\frac{N-1}{2}$  harmonic oscillators that are coupled only via the nonlinear trigger  $x_N$ , as will be shown in Section III (compare also [8]). For even  $N$ , the linear subsystem can be transformed into  $\frac{N-2}{2}$  oscillators together with one variable, which simply grows exponentially. That means, there is one positive real eigenvalue in addition to  $\frac{N-2}{2}$  pairs of complex conjugate eigenvalues. This leads to a qualitatively different dynamics. See the remark at the end of subsection IIIB for clarifying this point. In the present paper, we restrict ourselves to the case of odd  $N$ .

## III. THE MODE PICTURE

In the following section, we develop the mode picture of the GRS. First, we will present the solution of the linear subsystem. Herewith, we can transform the GRS into a mode picture, where the linear subsystem  $\mathbf{x}$  consists of harmonic oscillators, which are coupled only via the nonlinear trigger variable  $x_N$ . In the mode picture, we are in the position to explain the idea of the structural symmetry, which will be of central importance for understanding the dynamics of the GRS in subsequent sections. Finally, we show the fixed points together with their stability properties.

### A. Semianalytical solution of the linear subsystem

Consider the linear subsystem  $\mathbf{x}$  (Eq. (1)). Here, we restate the equations in component form as a linear chain with boundary conditions:

$$\begin{aligned} \frac{d}{dt}x_n &= x_{n-1} - x_{n+1}, \quad n \in \{1, \dots, N-1\}, \\ x_0 &= ax_1, \\ x_N &= 0. \end{aligned} \quad (3)$$

To solve the linear subsystem  $\mathbf{x}$ , an exponential ansatz is used:

$$\begin{aligned} x_{2n+1} &= \cos((2n+1)k + \varphi)e^{i\Omega(k)t}, \\ &\quad \text{for } n \in \{0, \dots, \frac{N-3}{2}\}, \\ x_{2n} &= c \sin(2nk + \varphi)e^{i\Omega(k)t}, \\ &\quad \text{for } n \in \{0, \dots, \frac{N-1}{2}\}, \end{aligned} \quad (4)$$

where  $k$  is the wave number of the eigenmodes,  $\Omega(k)$  the corresponding frequency with a specific dispersion relation. Substituting ansatz (4) into chain (3) yields

$$\begin{aligned} c &= -i, \\ \Omega_{\pm m} &= 2 \sin(k_{\pm m}), \quad m \in \{1, \dots, \frac{N-1}{2}\}, \\ k_{\pm m} &= \pm \frac{2m-1}{2N}\pi - \frac{1}{N}\varphi_{\pm m}, \\ -i \sin(\varphi_{\pm m}) &= a \cos(\pm \frac{2m-1}{2N}\pi + \frac{N-1}{N}\varphi_{\pm m}). \end{aligned} \quad (5)$$

These  $(N-1)$  eigenmodes are a complete solution of the  $(N-1)$  dimensional linear subsystem  $\mathbf{x}$  for odd  $N$ . The solution is analytical up to a complex correction  $\varphi_{\pm m}$  to the allowed wave numbers  $k_{\pm m}$ , which is determined by a transcendent equation. For  $a = 0$ , this equation can be solved giving

$$\begin{aligned} \varphi &= 0, \\ k &= \frac{2m-1}{2N}\pi, \quad \text{where } m \in \{1, \dots, \frac{N-1}{2}\}. \end{aligned} \quad (6)$$

For  $a < 1$ , there are  $\frac{N-1}{2}$  pairs of complex conjugate eigenvalues  $(\Omega_m, \Omega_{-m})$ , where  $\Omega_m = -\bar{\Omega}_{-m}$ . The corresponding pairs of eigenmodes represent harmonic oscillators with angular frequencies  $\omega_m = \text{Re } \Omega_m$  and autocatalytic coefficients  $\alpha_m = -2 * \text{Im } \Omega_m$ . The complex corrections  $\phi_{\pm m}$  to the values of  $k_m$  for  $a \neq 0$  can easily be expanded about  $a = 0$ . The expansion is up to the order of  $a^2$

$$\begin{aligned} \phi_{\pm m} &= ia \cos(\frac{2m-1}{2N}\pi) \\ &\quad + \frac{N-1}{2N}a^2 \sin(\pm \frac{2m-1}{N}\pi) + O(a^3). \end{aligned} \quad (7)$$

In the considered range of  $a \in [0, 0.35]$ , this is an excellent approximation (however, in the subsequent analysis, we have numerically calculated the eigenvalues and eigenvectors of  $\mathbf{A}$  in order to minimize errors). The imaginary part of  $\varphi_m$  determines the autocatalytic coefficient  $\alpha_m$ . It is linear in  $a$  up to  $O(a^3)$ . The real part leads to a correction of  $\omega_m$ . But for  $a \in [0, 0.35]$ , this correction is very small, i.e., the frequencies of the oscillators are almost independent of  $a$  in the considered range. From equation (5), we infer that the frequencies of the oscillators are bounded ( $0 < \omega < 2$  for all  $N$ ) and we expect the autocorrelation time  $\tau_c$  in the case of an unstable dynamics to be independent of  $N$ . Additionally, the velocity of signals of frequency  $\omega$  traversing the linear subsystem equals  $2 \cos k$ . Therefore, the time  $\tau_s$  a signal takes to traverse the linear subsystem (from  $x_1$  to  $x_{N-1}$ ) or back, since the linear subsystem allows for a bidirectional transport of signals) is expected to be approximately  $N/2$ .

### B. The mode transformation

We have solved the linear subsystem  $\mathbf{x}$ . The next step is to transform it into its eigensystem  $\mathbf{y}$ . The transformed equations for  $\mathbf{y}$  are completely decoupled (as the matrix  $\mathbf{A}$  is transformed into a diagonal matrix). Thus, we can treat the different oscillators independently. The idea of the following steps of the transformation is to bring the oscillators that correspond to pairs of complex conjugate eigenvalues into a form that is as similar to the oscillator of the original Rössler system as possible. The oscillators are of the form

$$\frac{d}{dt} \begin{pmatrix} y_{2m-1}(t) \\ y_{2m}(t) \end{pmatrix} = \begin{pmatrix} i\Omega_m & 0 \\ 0 & -i\Omega_m \end{pmatrix} \begin{pmatrix} y_{2m-1}(t) \\ y_{2m}(t) \end{pmatrix}.$$

It can be considered as the principal value decomposition of the following Rössler-like oscillator:

$$\frac{d}{dt} \begin{pmatrix} z_{2m-1}(t) \\ z_{2m}(t) \end{pmatrix} = \begin{pmatrix} -\alpha_m & -\omega_m^2 \\ 1 & 0 \end{pmatrix} \begin{pmatrix} z_{2m-1}(t) \\ z_{2m}(t) \end{pmatrix}.$$

In the following, these oscillators are called *oscillator*  $(z_{2m-1}, z_{2m})$ . For each variable of the linear subsystem  $\mathbf{x}$ , one can choose one complex factor of normalization. It can be utilized to make the entire transformation real (via phase factors) and to give the coupling to the nonlinearity  $x_N$  – which is not touched by the transformation – a certain form (via amplitude factors). We choose this coupling in such a way that the resulting equations are

$$\begin{aligned} \frac{d}{dt} \mathbf{z}(t) &= \mathbf{B} \mathbf{z}(t) - x_N(t) \mathbf{c} \\ \frac{d}{dt} x_N(t) &= \varepsilon + b x_N(t) \left( \sum_{m=1}^{\frac{1}{2}(N-1)} z_{2m} - d \right), \end{aligned} \quad (8)$$

where

$$\mathbf{B} = \begin{pmatrix} \alpha_1 & -\omega_1^2 & 0 & \cdots & 0 \\ 1 & 0 & & \ddots & \vdots \\ 0 & & \ddots & & 0 \\ \vdots & \ddots & & \alpha_{\frac{N-1}{2}} & -\omega_{\frac{N-1}{2}}^2 \\ 0 & \cdots & 0 & 1 & 0 \end{pmatrix}.$$

For the  $\alpha_m$ , it holds  $\sum_{m=1}^{\frac{1}{2}(N-1)} \alpha_m = a$ , as the divergence of the GRS is not affected by the transformation.  $\mathbf{c}$  denotes the vector of coupling constants of  $x_N$  to the components of  $\mathbf{z}$ . If the complete transformation is called  $\mathbf{U}$  (i.e.  $\mathbf{z} = \mathbf{U}^{-1} \mathbf{x}$ ), then the vector of coupling constants  $\mathbf{c}$  is  $\mathbf{c} = \mathbf{U}^{-1} \mathbf{e}_{N-1}$ . For  $a = 0$ , we have  $\mathbf{c} = \frac{1}{N} \left( 0, (\cos k_1)^2, 0, (\cos k_2)^2, \dots, 0, (\cos k_{\frac{N-1}{2}})^2 \right)^t$ . This *mode transformation* converts the GRS into a system of oscillators with frequencies  $\omega_m$  and autocatalytic coefficients  $\alpha_m$ , that are coupled solely via the nonlinear trigger  $x_N$ . The coupling has a special form: the oscillators couple to the trigger only with the sum of their variables  $z_{2m}$ , i.e., they couple to  $x_N$  identically. The coupling of  $x_N$  back to  $\mathbf{z}$  is different for the different oscillators. In the following, we call the original form of the GRS the *Baier-Sahle picture* and the transformed form the *mode picture*. In Fig. 1, the structures of the Baier-Sahle picture and the mode picture are compared. Each linear degree of freedom is represented by a circle, each nonlinear degree of freedom by a square. Couplings are shown as connecting lines. In the Baier-Sahle picture, the similarity of the GRS to a spatially extended system is most obvious: the autocatalytic process and the nonlinear trigger  $x_N$  can be considered as the boundary conditions of a homogeneous linear chain. On the other hand, in the mode picture, the dynamics of the GRS can be understood as the interaction of different oscillators, that are coupled only via one nonlinear trigger. As the trigger  $x_N$  influences the dynamics of the linear subsystem only during the presence of the spikes, the effect of coupling is restricted to these short intervals in time. This allows to observe the dynamics of the different oscillators independently in the respective projections of phase space (see Section IV).

For even values of  $N$ , one finds one positive real eigenvalue of the linear subsystem for  $a > 0$ . In the mode picture, this corresponds to one exponentially growing degree of freedom, which is coupled to the nonlinear trigger  $x_N$  in the same way as the even coordinates of the oscillators. The contribution of the nonlinear trigger to the time derivative of this exponential mode is always negative. Thus, if once the exponential mode is pushed to a negative value by the nonlinear trigger it will escape to  $-\infty$ . This mechanism, in general, leads to a global instability of the GRS for even  $N$ .

### C. The structural symmetry

The mode picture reveals the GRS to consist of harmonic oscillators  $(z_{2m-1}, z_{2m})$ , that are identically coupled to the nonlinear trigger  $x_N$  (compare Fig. 1). A perfectly symmetric system of the same structure as that in Fig. 1(b), i.e., one with identical coefficients for each oscillator, would be symmetric with respect to any permutation of the oscillators. The invariant manifolds of such a system, specifically, the orbits and attractors, would have to obey this symmetry. For the invariant manifolds, there are two possibilities. Either they show the full symmetry in themselves, i.e., they are symmetric with respect to any permutation of the oscillators. Or they have coexisting mirror images,

such that the union of them obeys the full symmetry. In the GRS, the symmetry is broken merely by the difference in the frequencies  $\omega_m$ , autocatalytic coefficients  $\alpha_m$ , and coupling constants  $c_n$ . Nevertheless, the symmetry is preserved as a qualitative feature of the dynamics, as will be shown later on. We call this property *structural symmetry*. For arbitrary odd  $N$ , the structural symmetry will be utilized to understand and predict number, shape, and location of the attractors of the GRS in phase space for moderate values of the autocatalytic coefficient  $a$ . The first manifestation of the structural symmetry can be seen in the stability properties of the fixed points of the GRS.

#### D. The fixed points

The fixed points of a dynamical system are the pivots around which the system evolves. Thus, it is essential to investigate the stability properties of the fixed points, if one wants to develop any understanding of a dynamical system. For odd  $N$ , the GRS has two fixed points which are the same in all odd dimensions  $N$ , in the sense that the common linear coordinates and the nonlinear coordinate are identical for any two GRSs of different  $N$ . The two fixed points are (for odd  $N$ )

$$\begin{aligned} x_1^{(1,2)} &= x_3^{(1,2)} = \dots = x_N^{(1,2)} \\ &= \frac{d}{2a} \mp \sqrt{\left(\frac{d}{2a}\right)^2 - \frac{\varepsilon}{ab}} , \\ x_2^{(1,2)} &= x_4^{(1,2)} = \dots = x_{N-1}^{(1,2)} \\ &= \frac{d}{2} \mp \sqrt{\left(\frac{d}{2}\right)^2 - \frac{\varepsilon a}{b}} . \end{aligned} \quad (9)$$

Here, the minus signs belong to the index (1). The fixed point  $(\mathbf{x}^{(1)}, x_N^{(1)})$  lies close to the origin of the system (for  $\varepsilon = 0$ , it would be the origin). Accordingly, the stability analysis of this fixed point yields, in good approximation, the eigenmodes of the linear subsystem. The additional  $N$ -th eigenvalue is strongly attractive. It corresponds to the exponential decay of  $x_N$  to  $\frac{\varepsilon}{bd - x_{N-1}}$  and its value is approximately  $-bd$ , as is to be expected. On the unstable manifold of this fixed point, the GRS expands until it is folded back by a trigger event of  $x_N$ . The presence of the nonlinear trigger  $x_N$  slightly stabilizes the eigenmodes, such that they do no longer become unstable at  $a = 0$ , but approximately at  $a = 0.006$ . Interestingly, the oscillators that become unstable first are the ones that have a larger autocatalytic coefficient  $\alpha_n$  for higher values of  $a$  (see Fig. 2).

At the fixed point  $(\mathbf{x}^{(1)}, x_N^{(1)})$ , one can already perceive the fingerprint of the structural symmetry: for each oscillator of the GRS, there is an oscillatory instability of the inner fixed point  $(\mathbf{x}^{(1)}, x_N^{(1)})$ . The symmetry breaking is responsible for the difference in the eigenvalues of the fixed point. It will be shown in Section IV that each of these instabilities of the fixed point  $(\mathbf{x}^{(1)}, x_N^{(1)})$  gives rise to a coexisting attractor of the GRS. The fixed point  $(\mathbf{x}^{(2)}, x_N^{(2)})$  governs the folding process of the GRS. However, none of the attractors ever comes close to this fixed point.

### IV. DYNAMICS OF THE GENERALIZED RÖSSLER SYSTEM IN PHASE SPACE

In the following section, the mode picture and the concept of structural symmetry will be utilized to develop an understanding of the dynamics of the GRS in the  $N$ -dimensional phase space. At first, we discuss the case  $N = 5$  in some detail. It will be demonstrated that for values of  $a < 0.09$  two attractors coexist. For higher values of  $a$ , they interact in several crises. Finally, the two attractors merge into one hyperchaotic attractor. This scenario of three parameter regimes of coexisting attractors, interacting attractors, and one large hyperchaotic attractor will then be shown to hold in the case  $N = 7$  as well. Finally, we postulate that the dynamics of the GRS in arbitrary odd dimension  $N$  can be explained by extrapolating this scheme. For all numerical calculations, we have restricted ourselves to the variation of  $N$  and  $a$ . The other parameters remain constant at the values  $\varepsilon = 0.1$ ,  $b = 4$ ,  $d = 2$ .

#### A. Numerical study of the case $N = 5$

In the mode picture, the five-dimensional GRS consists of two oscillators that are coupled via the nonlinear trigger. First, we present a bifurcation diagram (Fig. 3) and the corresponding Lyapunov spectrum (Fig. 4) under variation of the control parameter  $a$  (see Appendix for the numerical methods that were used). The bifurcation diagram consists of two separate parts. They correspond to two coexisting attractors and have been obtained using different initial conditions.

As one increases  $a$  from  $a = 0$ , the fixed point near the origin becomes unstable at about  $a = 0.0006$ . Shortly one after the other, the two attractors emerge in two subsequent Hopf bifurcations as limit cycles. These two periodic orbits constitute the basis for all further development of the attractors. Although they become unstable at some point, they exist up to the highest values of  $a$ . In the following, they will be referred to as the *period-1 limit cycles* of the two attractors. *Attractor 1* develops as a result of the instability that corresponds to oscillator  $(z_1, z_2)$  in the mode picture. Accordingly, *attractor 2* develops out of  $(z_3, z_4)$ . In Fig. 5, two phase space projections of the period-1 limit cycle of attractor 1 are shown: one onto oscillator  $(z_1, z_2)$  together with the nonlinear trigger variable  $x_5$  and the other onto oscillator  $(z_3, z_4)$  together with  $x_5$ . The amplitude of oscillator  $(z_3, z_4)$  is negligible compared with that of oscillator  $(z_1, z_2)$ . Here, the dynamics of the GRS is completely dominated by  $(z_1, z_2)$  together with  $x_5$ . In general, the frequencies of the two oscillators are incommensurate. The two oscillators drift out of phase in each revolution. However, the spikes in  $x_5$  cause phase shifts in  $(z_3, z_4)$  that resynchronize the two oscillators. This leads to a 1:2 mode locking. For higher  $a$  (i.e., above  $a = 0.05$ ), oscillator  $(z_1, z_2)$  can no longer force the phase locking and the periodic orbit breaks up into a quasiperiodic one. As one increases  $a$  further, attractor 1 shows several periodic windows and, finally, low-dimensional chaos arises. In Fig. 6, the phase space projections of this low-dimensional chaotic form of attractor 1 are depicted. Oscillator  $(z_3, z_4)$  has still a much smaller amplitude than oscillator  $(z_1, z_2)$  (though its influence on the nonlinear trigger  $x_5$  is no longer negligible). And, remarkably, the dynamics in the three-dimensional projection onto  $(z_1, z_2)$  together with  $x_5$  shows a close resemblance to the Rössler system. It, therefore, can be considered as a 'perturbed' Rössler system.

The evolution of attractor 2 under variation of  $a$  is completely analogous, except that now oscillator  $(z_3, z_4)$  plays the dominant role and  $(z_1, z_2)$  is very small. In Fig. 7, the period-1 limit cycle of attractor 2 is depicted. It corresponds to the periodic orbit of attractor 1 shown in Fig. 5. Here, oscillator  $(z_3, z_4)$  is dominant, whereas oscillator  $(z_1, z_2)$  has a negligible amplitude. The phase locking between the oscillators is accomplished by phase shifts in oscillator  $(z_1, z_2)$  due to the spikes in  $x_5$  which are in turn triggered by  $(z_3, z_4)$ . Again, the dynamics in the projection, here onto  $(z_3, z_4)$  together with  $x_5$ , resembles that of the Rössler system, which can best be seen on the low-dimensional chaotic orbit in Fig. 8 (compare the chaotic orbit on attractor 1 in Fig. 6).

The existence of the two attractors is a consequence of the structural symmetry: in a perfectly symmetric system (of the same structure as the GRS in the mode picture), each attractor, that is not in itself symmetric with respect to the exchange of any two oscillators (i.e., the transformation  $z_1 \leftrightarrow z_3, z_2 \leftrightarrow z_4$  in the case  $N = 5$ ), must necessarily have one or more mirror images, such that their union fulfills the symmetry. An attractor, where oscillator  $(z_1, z_2)$  dominates oscillator  $(z_3, z_4)$ , is obviously not symmetric with respect to the above transformation. Therefore, in the perfectly symmetric system, there would have to be another coexisting attractor, where oscillator  $(z_3, z_4)$  dominates oscillator  $(z_1, z_2)$ . In the GRS, the symmetry is broken by the difference in the frequencies, autocatalytic constants, and coupling constants. However, as has been shown above, these two attractors do still exist. Moreover, their shape and location in phase space does, indeed, reflect the structural symmetry. Attractor 1 lies close to the subspace defined by  $z_3 = 0$  and  $z_4 = 0$ . Attractor 2 is situated close to the subspace defined by  $z_1 = 0$  and  $z_2 = 0$ . On attractor 1, oscillator  $(z_1, z_2)$  is dominant and, on the periodic orbits, the phase locking is kept up by phase shifts of oscillator  $(z_3, z_4)$ . On attractor 2, accordingly, oscillator  $(z_3, z_4)$  is dominant and, on the periodic orbits, the phase locking is kept up by phase shifts of oscillator  $(z_1, z_2)$ .

Up to  $a \simeq 0.09$ , the two attractors develop independently. They are located clearly separate in phase space. Then, a boundary crisis occurs: Attractor 1 collides with the separatrix to the basin of attractor 2 and ceases to exist as a stable dynamical state. It still attracts the trajectories out of its basin, but eventually every trajectory ends up in attractor 2. At  $a \simeq 0.115$ , another crisis can be observed. In the bifurcation diagram (Fig. 3), the dynamics on the resulting attractor resembles that of attractor 1. However, it is not at all obvious, whether it is, indeed, attractor 1 or, maybe, the two attractors merged. In order to answer this question, we select an initial condition on the period-1 orbit of "attractor 2" and observe how the GRS develops from there. For this purpose, we utilize the time-delayed feedback control method introduced by Pyragas [9] (see Appendix, for the utilized numerical algorithm). With the aid of the control, we force the GRS onto the period-1 orbit of "attractor 2" (Fig. 7) at  $a = 0.12$  (see Fig. 9). It should be remarked here that, in a strict sense, one can no longer talk of the "attractor" after it has undergone a boundary crisis. However, as it still attracts the trajectories of its basin and the transient motion along them may be very long, we will, nevertheless, still call it attractor. The fact that this is possible (with vanishing control signal) demonstrates, that at least the period-1 limit cycle of attractor 2 does still exist. Subsequently, we switched off the control. First, the trajectory left the unstable periodic orbit according to the largest Lyapunov exponent of that orbit. Then, it remained on attractor 2 for approximately 1000 revolutions. But, eventually, the trajectory changes very quickly to an attractor-1-type shape and, within the patience of the authors (for a relatively long time interval of  $\Delta t = 300000$ , i.e., about 30000 revolutions), it never again showed attractor-2-type behavior (Fig. 10). From this, we conclude that the attractor at  $a = 0.12$  is, indeed, attractor 1 and attractor 2 has lost its stability. In order to arrive at this situation, two things must have happened: attractor 2 must have undergone a boundary crisis into the basin of attractor 1 and attractor 1 must have separated from the separatrix in an inverse boundary crisis. It seems virtually

impossible that these two incidents occur at the same value of  $a$ . Thus, depending on the order they occur, there should be a small interval of either coexisting or merged attractors in between. There is some numerical evidence that, indeed, the second situation is valid.

The development of the two attractors as a function of  $a$  can also be observed in the Lyapunov exponents. Figure 4 shows the Lyapunov exponents of attractor 1 except for the interval  $a \in [0.9, 0.115]$ , where attractor 1 does not exist. The sequence of periodicity, quasiperiodicity with periodic windows, and chaos can clearly be seen. For  $a > 0.115$ , the GRS is hyperchaotic [6]. In Fig. 11, the phase space projections of the hyperchaotic attractor at  $a = 0.3$  are shown. Interestingly, the second Lyapunov exponent becomes positive in the vicinity of the second and the third crisis. From that point, the three largest Lyapunov exponents grow more or less linearly with  $a$  (except for a small periodic window at  $a \simeq 0.23$ ). The GRS in this range of  $a$  can no longer be regarded as a perturbed Rössler system in any projection. Oscillator  $(z_1, z_2)$  gradually ceases to be dominant and the dynamics of the GRS seems more and more irregular. At  $a \simeq 0.17$ , the third Lyapunov exponent becomes positive. The Lyapunov dimension of the attractor is larger than 4. However, no qualitative change of the dynamics could be observed at this point, either in the bifurcation diagrams or in the phase space projections.

## B. Numerical study of the case $N = 7$

We now proceed to show that the GRS does behave in a similar manner in the case  $N = 7$ . In the mode picture, the seven-dimensional GRS consists of three oscillators coupled via the nonlinear trigger  $x_7$ .

If one compares the bifurcation diagram (Fig. 12) and the corresponding Lyapunov spectrum (Fig. 13) with those of  $N = 5$  (Figs. 3 and 4, respectively), one perceives a striking resemblance. There are three coexisting attractors for lower  $a$  ( $a \in [0, 0.05]$ ), corresponding to the three oscillators of the seven-dimensional GRS. Two of these attractors vanish via boundary crises in an intermediate regime of interacting attractors ( $a \in [0.06, 0.115]$ ). Finally, only one attractor remains, which is hyperchaotic with an increasing number of positive Lyapunov exponents.

For  $a \in [0, 0.05]$ , each of the three attractors can be characterized by the dominance of one of the three oscillators. Each attractor develops as a result of the instability of the fixed point  $(\mathbf{x}^{(1)}, x_N^{(1)})$  corresponding to the respective dominant oscillator. This oscillator triggers  $x_7$ , while the other two oscillators have a small amplitude. On *attractor 1*, oscillator  $(z_1, z_2)$  is dominant, on *attractor 2*, oscillator  $(z_3, z_4)$ , and on *attractor 3*, oscillator  $(z_5, z_6)$ . As long as the attractors are periodic (e.g., for  $a \in [0.006, 0.04]$  on attractor 1) the mode locking is kept up by phase shifts in the two oscillators with the small amplitude as in the case  $N = 5$ . Most remarkably, on all three attractors, the dynamics is qualitatively equal to that of the Rössler system in the projection onto the respective dominant oscillator together with the nonlinear variable  $x_7$ , i.e., in a three-dimensional phase space (compare Fig. 14 (a) and (b) for the period-1 orbit on attractor 2, and Fig. 14 (c) and (d) for a chaotic orbit on attractor 2). Again, the existence, form, and location in phase space of the three attractors can be interpreted as a manifestation of the structural symmetry. They appear as mirror images of each other under the symmetry operation of an exchange of the dominant oscillator with one of the other oscillators. For example, attractor 1 would be obtained from attractor 2 by the transformation  $z_1 \leftrightarrow z_3, z_2 \leftrightarrow z_4$ .

For small values of  $a$ , the dominant oscillator of each of the attractors has a large amplitude, while the other two oscillators remain small. That means, the three attractors are located in phase space close to the subspace of the respective dominant oscillator together with the nonlinear trigger  $x_7$ . Thus, they are clearly separate from each other. With increasing  $a$ , the attractors grow and begin to interact. First, attractor 3 vanishes at  $a \simeq 0.052$  in a boundary crisis, where it collides with the separatrix to the basin of attractor 1. Attractor 1 also loses stability at  $a \simeq 0.06$ , such that only attractor 2 remains stable. Finally, at  $a = 0.11$ , a third crisis occurs, which leaves a large attractor that encompasses the dynamics of all three attractors. In general, the motion from one attractor to the other is much slower than the motion on the attractors (compare Fig. 10).

In Fig. 13, the Lyapunov exponents as a function of  $a$  are shown. For  $a < 0.06$ , the GRS is on attractor 1. In the grey-shaded region  $a \in [0.06, 0.115]$ , the GRS revolves on attractor 2. For  $a > 0.115$ , the Lyapunov exponents of the remaining hyperchaotic attractor can be seen. Here, the Lyapunov exponents grow approximately linear with  $a$ , similar to the case  $N = 5$ .

## C. Dynamics for arbitrary odd dimension $N$

We have demonstrated how the dynamics of the GRS in the cases  $N = 5$  and  $N = 7$  can be understood within the same scheme of coexisting attractors. We expect that the dynamics of the GRS behaves in an analogous way for every odd dimension  $N$ . Thus, we expect, in general,  $\frac{N-1}{2}$  coexisting attractors for small values of  $a$ . On each of the

attractors, one of the oscillators of the mode picture will be dominant. Each attractor will be located close to the hyperplane of the respective dominant oscillator together with the nonlinear trigger. The other oscillators will have a negligible amplitude. In the projection onto the dominant oscillator together with the nonlinear trigger  $x_N$ , the dynamics will be Rössler-like. For higher values of  $a$ , the attractors will grow in phase space and interact with each other in several crises. Eventually, one hyperchaotic attractor will remain, which extends over all of the phase space that was occupied by the  $\frac{N-1}{2}$  coexisting attractors.

For clarity, we shortly discuss the dynamics of the GRS in phase space for a higher number of variables,  $N = 61$ . To this end, we use a pseudo space-time representation of the dynamics in Fig. 15 for three different values of  $a$ . The values of every second variable  $x_{2n+1}, n = 0, \dots, 30$ , are depicted in grey scale as a function of time. In order to ensure that the dynamics has settled on the attractor, the GRS was propagated for a transient time 500000, which corresponds to about 10000 revolutions of the slowest oscillator for  $N = 61$ . A periodic orbit for  $a = 0.04$  is visualized in Fig. 15(a). In the mode picture, the mean amplitudes of the five dominant oscillators are: 1.30, 1.16, 1.12, 0.40, 0.11, 0.05, 0.04. The amplitudes of the other oscillators are smaller than 0.01. Obviously, the dynamics is not dominated by a single oscillator, suggesting that the coexisting periodic orbits have undergone one or more merging crises before losing their stability. In Fig. 15 (b), a comparatively low-dimensional chaotic orbit close to the above periodic one (Fig. 15(b)) is shown. It has been calculated for  $a = 0.07$ . The trace of the periodic orbit can still be seen in the image. Additionally, a considerable activity of high-frequency modes can be perceived as well. The largest Lyapunov exponents are: 0.00021, 0.00017, 0.00014, 0.00010, 0.00009, 0.00008, 0.00008, 0.00002, 0.00001,  $-0.00001$ ,  $-0.00003$ ,  $-0.00005$ . From this, the Lyapunov dimension is estimated to be  $D = 20.8$  with the help of the Kaplan-Yorke conjecture [10]. In this state, the GRS does not explore all of its phase space and several other coexisting chaotic attractors can be found, which are not shown here. Figure 15(c) shows a snapshot for  $a = 0.15$ , which lies in the hyperchaotic regime. Here, no coherent structure can be perceived. This state has 38 positive Lyapunov exponents and a Lyapunov dimension of  $D = 60$ . In this state, the hyperchaotic attractor extends to all of the phase space and no coexisting attractor can be found.

For large values of  $N$ , the GRS is similar to a time delay system of the form  $\dot{y}(t) = f(y(t - \tau)) + g(y(t))$ , as investigated ,e.g., in [11–17]. This can clearly be seen in Fig. 15. The linear subsystem  $\mathbf{x}$  acts as a delay-line, that merely transports signals back and forth between the positive feedback process, represented by  $x_1$ , and the nonlinear trigger  $x_N$ . The delay time of the GRS is approximately  $N$  (see III A). The difference between the GRS and a time delay system is that the GRS – as a spatially discrete system – has got a nonlinear dispersion relation  $\omega(k)$ . As every mode of the GRS is active for values of  $a$  in the hyperchaotic regime, the dispersion relation cannot be neglected in that case. Thus, the function  $f$  would have to be replaced by a functional in  $y(t - \Delta t)$  with  $\Delta t > N$ . Still, the GRS has got the same basic structure as a time delay system. We arrive at identical scaling properties of the Lyapunov exponents, the Lyapunov dimension, and the metric entropy for  $N \rightarrow \infty$ , as will be shown in the following section.

## V. PROPERTIES OF THE GENERALIZED RÖSSLER SYSTEM UNDER VARIATION OF SYSTEM SIZE $N$

Up to now, we have investigated the dynamics of the GRS in phase space under variation of the control parameter  $a$  for the cases  $N = 5$  and  $N = 7$ . In the present section, we investigate the GRS as a function of  $N$  for four fixed values of  $a$ :  $a = 0.3, a = 0.25, a = 0.15$ , and  $a = 0.07$ . The first three values of  $a$  are in the regime of large, phase-space filling hyperchaotic attractors, the fourth value of  $a$  lies in the regime of low-dimensional, coexisting attractors.  $N$  is varied from 3 to 61. Here, we mainly focus on the numerical calculation of Lyapunov exponents, from which the Lyapunov dimension  $D_\lambda$  and the metric entropy  $H$  are estimated. The Lyapunov exponents have been calculated with the fixed initial condition  $(\mathbf{x}, x_N) = (1, 0, \dots, 0, 0)$ . The other parameters are again chosen to be  $\varepsilon = 0.1$ ,  $b = 4$ , and  $d = 2$ . Interpreting the dimensionality  $N$  of the GRS as system size, we compare the results to the ‘thermodynamic limes’ of homogeneous, spatially extended systems, where the number of positive Lyapunov exponents, the Lyapunov dimension, and the metric entropy are reported to be proportional to  $N$  [18–22]. In this case, the distribution of Lyapunov exponents has been reported to approach a limit function  $f$ , i.e.,  $\lambda_i = f(i/V)$ , if  $V$  is the system size [23]. In the next step, we draw the attention to the GRS’s similarity to time-delay systems, where the Lyapunov dimension has been reported to be proportional to the delay time, while the metric entropy approaches a limit value for increasing delay time [11].

Figure 16 shows the number of positive Lyapunov exponents  $N^+$ , the Lyapunov dimension  $D_\lambda$  (estimated via the Kaplan-Yorke relation [10]) and the metric entropy  $H$  (estimated via the Pesin formula [24]) as a function of  $N$  for the four values of  $a$ . The number of positive Lyapunov exponents  $N^+$  and the Lyapunov dimension  $D_\lambda$  grow linearly with  $N$ . Remarkably, the Lyapunov dimension  $D_\lambda$  is maximal up to its fractional part (i.e.,  $D_\lambda > N - 1$ ) for almost all odd dimensions  $N$ , as long as the GRS is in the hyperchaotic regime (large enough  $a$ ). The metric entropy approaches



a limit value  $H_\infty$  for large  $N$ . Therefore, the Lyapunov exponents decrease proportional to  $1/N$ . Note that this observation is not so clear-cut for  $a = 0.07$ , probably due to the fact that the chosen initial condition lies within the basin of attraction of different attractors for different values of  $N$ . Therefore, we find that the limit  $N \rightarrow \infty$  of the GRS is similar to the limit of an increasing delay time of time-delay systems and is not similar to the 'thermodynamic limit' of homogeneous, spatially extended systems. Recently, the constancy of the metric entropy of time-delay systems for increasing delay time has been attributed to the constancy of the number of 'localized nonlinearities' [17]. The same idea applies to the GRS. In Section II, we have distinguished between a linear,  $(N - 1)$ -dimensional subsystem  $(x_1, \dots, x_{(N-1)})$  and a one-dimensional nonlinear subsystem (the trigger variable  $x_N$ ). The linear subsystem  $(x_2, \dots, x_{(N-1)})$  (without the positive feedback process present in  $x_1$ ) allows only for a linear, bi-directional transport of signals and is, therefore, not able to initiate any unstable behavior (see Fig. 15). In the case of the GRS, it is the one-dimensional 'localized nonlinearity'  $x_N$  [17] (together with  $x_1$ ), which allows for a nonlinear stretching and folding in phase space and is solely responsible for the positive metric entropy. As in the case of time-delay systems, we expect the value of the metric entropy  $H$  for increasing  $N$  to depend only on the number of localized nonlinearities, which is equal to one for the GRS, and the rate with which the information is processed, which is estimated via the correlation time  $\tau_c$ . Therefore, we hypothesize that the metric entropy scales like

$$H \propto \frac{1}{\tau_c}, \quad (10)$$

for  $N \rightarrow \infty$ . Since in the hyperchaotic case the correlation time is expected to be independent of  $N$  (see Sec. III.A), eq. (10) reproduces the limit behavior of the metric entropy of the GRS. In the case of homogeneous, spatially extended systems, we expect the number of localized nonlinearities to increase proportional with the system size. This leads to a proportional increase of the metric entropy with the system size, as has been observed in several models.

Thus, we conjecture that the high-dimensional chaotic motion observed in the GRS is fundamentally different compared to the spatio-temporal chaos observed in homogeneous, spatially extended systems. Here, the difference is expressed in terms of the number of localized nonlinearities a system possesses in phase space. In the case of the GRS, the number of the localized nonlinearities is independent of the control parameters including the system size. In the case of homogeneous and nonlinear spatially extended systems, the number of localized nonlinearities is expected to grow proportional to the system size.

In Table I, we show the limit value  $H_\infty$  for different values of  $a$ . Additionally, the value of  $H_\infty$  normalized to the autocatalytic coefficient  $a$  is shown. Note that the value of  $a$  is an upper bound for the sum of the positive Lyapunov exponents and, with this, to the estimated metric entropy  $H$ . The case  $a = H_\infty$  corresponds to an unbounded, linear,  $(N - 1)$ -dimensional system,  $(x_1, x_2, \dots, x_{N-1})$  in absence of the localized nonlinearity  $x_N$ .

From Table 1, we infer that the limit value of the metric entropy,  $H_\infty$ , comes closer to its upper bound  $a$  for an increasing value of  $a$ , indicating that the hyperchaotic attractors increasingly exploit all the unstable directions available.

In the following, we examine the distribution of Lyapunov exponents as a function of  $N$ . If one is to compare the Lyapunov exponents of different systems, one faces the problem that the absolute values of them depend on the chosen time scale. In systems with many different characteristic times, like the GRS, it is not obvious which time scale to use. Above, the time scale for the GRS under variation of  $N$  has been chosen such that the highest frequency of the linear subsystem  $\omega_{max}$  is approximately equal to 2.0 (see eq. (5)). In this case, we expect the correlation time  $\tau_c$  to be approximately constant for different values of  $N$ , while the time  $\tau_s$  a signal needs to traverse the linear subsystem  $(x_1, \dots, x_{(N-1)})$  increases proportional to  $N$ . In the analysis to follow, we choose the time scale such that the rescaled mean positive Lyapunov exponent is equal to one. The rescaled Lyapunov exponents  $\lambda_s$  are defined as

$$\lambda_s = \frac{N^+}{\sum \lambda^+} \lambda, \quad (11)$$

where  $\sum \lambda^+$  denotes the sum over the positive Lyapunov exponents, i.e., the metric entropy, and  $N^+$  denotes the number of positive Lyapunov exponents. Using the time scale according to eq. (11), the maximal frequency of the GRS scales like  $\omega_{max} \approx 2 \frac{N^+}{H}$ . Assuming  $N^+ \approx N$  and  $H \rightarrow H_\infty$  for high enough  $a$ , we find  $\omega_{max} \propto \frac{N}{H_\infty}$ . From this the correlation time is estimated to decrease with  $N$  in the hyperchaotic case like  $\tau_c \propto \frac{H_\infty}{N}$ . The same argument applies to the scaling of the velocity of signals yielding  $v \propto \frac{N}{H_\infty}$ . This leads us to observe that the rescaling of the time according to eq. (11) makes the time  $\tau_s = N/v$  a signal needs to traverse the linear subsystem independent of the system size  $N$  for sufficiently large values of  $a$ .

In Fig. 17, the distribution of the rescaled Lyapunov exponents is shown for different values of  $N$  for  $a = 0.25$ . The Lyapunov exponents are sorted in descending order. The distributions converge to a limit distribution,  $\lambda_{s,i} = f(i/N)$ , with increasing  $N$ . We observe qualitatively the same behavior for all values of  $a$ . Note that, although the existence

of a limit distribution  $f$  has also been shown for homogeneous, spatially extended systems, the limes of an increasing system size  $N$  for the rescaled Lyapunov exponents (11) is considerably different from the thermodynamic limes of spatially extended systems. In the latter case, the correlation time is approximately independent of the system size, while in the case of the GRS the correlation time decreases proportional to the system size  $N$ .

In delayed dynamical systems with an expansive local dynamics (local in time), there has been reported the existence of “anomalous” Lyapunov exponents [25,15] which do not scale like  $1/N$  for  $N \rightarrow \infty$ , but remain at a finite value. Considering the similarity of the GRS with a delayed system and the expansive term present in  $\dot{x}_1 = ax_1 - x_2$ , one may expect to observe such an anomalous Lyapunov exponent for  $a > 0$ . However, due to the fact that the linear subsystem transports energy (in the form of squared amplitudes) away from  $x_1$ , the local dynamics of the beginning of the linear subsystem is that of a damped oscillator for all values of  $a$  considered in this paper. For values of  $a$  being sufficiently large such that the local dynamics does indeed become expansive, the GRS is globally unstable, as the nonlinear trigger is no longer able to keep the amplitudes of the linear subsystem bounded. Accordingly, no sign of an anomalous Lyapunov exponent (i.e., a Lyapunov exponent that does not scale like  $1/N$ ) could be seen in any of the spectra calculated for the present work.

Finally, we would like to discuss the shape of the limit distribution  $f$  of the rescaled Lyapunov exponents. We have observed above that the limit value of the metric entropy,  $H_\infty$ , approaches its upper bound  $a$  for an increasing value of  $a$  as a direct consequence of the dynamics increasingly exploiting all unstable directions of the unstable fixed point  $(\mathbf{x}^{(1)}, x_N^{(1)})$ . We find that the same idea applies to the Lyapunov spectra: For an increasingly hyperchaotic attractor (increasing value of  $a$ ), the Lyapunov spectra gain similarity with the real parts of the eigenvalues of the unstable fixed point  $(\mathbf{x}^{(1)}, x_N^{(1)})$ . In Fig. 18, we show the Lyapunov spectra for three different values of  $a$  (fixed dimension  $N = 61$ ) together with the real parts of the eigenvalues of the fixed point according to eq. (5). In all cases, the time scale has been chosen such that the trace of the matrix  $A$  equals one.

## VI. DISCUSSION AND CONCLUSION

We have investigated the GRS as a model for high-dimensional chaos as the latter emerges out of low-dimensional chaos. One important feature of the GRS is that it consists of a linear subsystem with a variable number of degrees of freedom together with one nonlinear trigger. The linear subsystem can be solved analytically. Utilizing the eigenmodes of the linear subsystem, one can transform the GRS into a mode picture, consisting of harmonic oscillators that are coupled only via the nonlinear trigger. The mode picture reveals a structural symmetry of the GRS. With the aid of this structural symmetry, we interpret the dynamics of the cases  $N = 5$  and  $N = 7$  within a general scheme of coexisting attractors. For small values of  $a$ , there is, for each attractor, a specific projection into a three-dimensional subspace, where the dynamics of the GRS is Rössler-like. The attractors expand with increasing  $a$  and interact in several crises. This parameter regime of interacting attractors eventually leaves one large hyperchaotic attractor with many positive Lyapunov exponents. Even such kind of hyperchaotic dynamics can be made accessible to the human mind, which is used to envisage in three spatial dimensions, with the help of three-dimensional projections onto the oscillators of the mode picture.

In the second part of this paper, we have investigated the Lyapunov exponents and related chaotic indicators of the GRS in the limit of large values of  $N$ , mainly in the hyperchaotic regime. The number of positive Lyapunov exponents and the Lyapunov dimension grow linearly with  $N$ . The Lyapunov dimension is maximal,  $D_\lambda \approx N$ , independently of  $a$ , as long as one is in the hyperchaotic regime. The metric entropy converges to a limit value for increasing  $N$ . If the time is rescaled in such a way that the signal travelling time through the linear subsystem remains constant with increasing  $N$ , the distribution of the Lyapunov exponents approaches a limit function and the metric entropy grows linearly with  $N$  for  $N \rightarrow \infty$ . We have argued that the hyperchaotic dynamics observed in the GRS is fundamentally different from spatio-temporal chaos. In this paper, we have expressed this difference in terms of the number of localized nonlinearities.

In Section I, we have raised the question how dynamical systems develop from low-dimensional chaotic behavior to hyperchaotic states. In the GRS, one observes one specific path through the chaotic hierarchy, starting from a stable fixed point over chaos up to hyperchaos. The GRS exhibits a scenario of coexisting Rössler-like attractors that interact and eventually merge to form a hyperchaotic attractor. We would like to emphasize that the GRS only realizes one possible way, ending up with one special form of hyperchaos. We feel that there are many different forms of hyperchaos which possibly cannot be sufficiently characterized with the help of Lyapunov exponents. In the case of the GRS, the structure of the system has provided a helpful scheme to interpret the dynamics. We believe that the investigation of the topological structure of the flow and, specifically, the attractor structure and the interaction of attractors, could be used to classify high-dimensional chaotic dynamics in general.

## ACKNOWLEDGEMENTS

We thankfully acknowledge fruitful discussions with G. Baier, S. Sahle, J. Peinke, and O.E. Rössler. The valuable contribution of the referee is worth mentioning. The present work has been supported financially by the Deutsche Forschungsgemeinschaft.

- 
- [1] E. N. Lorenz, J. Atmosph. Sc. **20**, 130 (1963).
  - [2] O. E. Rössler, Phys. Lett. **A 57**, 397 (1976).
  - [3] V. Jirsa, R. Friedrich, and H. Haken, Physica **D 89**, 100 (1995).
  - [4] O. E. Rössler, Z. Naturforsch. **38a**, 788 (1983).
  - [5] M. Klein and G. Baier, in *A Chaotic Hierarchy*, edited by M. Klein and G. Baier (World Scientific, Singapore, 1991), p. 1.
  - [6] O. E. Rössler, Phys. Lett. **A 71**, 155 (1979).
  - [7] G. Baier and S. Sahle, Phys. Rev. **E 51**, 2712 (1995).
  - [8] T. Meyer, M. J. Bünner, A. Kittel, and J. Parisi, Z. Naturforsch. **50 a**, 1135 (1995).
  - [9] K. Pyragas, Phys. Lett. **A 170**, 421 (1992).
  - [10] J. Kaplan and J. Yorke, in *Functional differential equations and approximations of fixed points*, Vol. 730 of *Lecture Notes in Math.*, edited by H.-O. Peitgen and H.-O. Walther (Springer, Berlin, 1979), p. 204.
  - [11] J. D. Farmer, Physica **D 4**, 366 (1982).
  - [12] G. Giacomelli, R. Meucci, A. Politi, and F. Arecchi, Phys. Rev. Lett. **73**, 1099 (1994).
  - [13] K. Ikeda and K. Matsumoto, J. Stat. Phys. **44**, 955 (1986).
  - [14] K. Ikeda and K. Matsumoto, Physica **D 29**, 223 (1987).
  - [15] G. Giacomelli, S. Lepri, and A. Politi, Phys. Rev. **E 51**, 3939 (1995).
  - [16] M. Bünner, T. Meyer, A. Kittel, and J. Parisi, to be published in Phys. Rev. **E**.
  - [17] M. Bünner, T. Meyer, A. Kittel, and J. Parisi, to be published in Z. Naturforsch. **a**.
  - [18] Y. Pomeau, A. Pumar, and P. Pelce, J. Stat. Phys. **37**, 39 (1984).
  - [19] R. Livi, A. Politi, and S. Ruffo, J. Phys. **A 19**, 2033 (1986).
  - [20] D. A. Egolf and H. S. Greenside, Nature **369**, 129 (1994).
  - [21] T. Bohr, E. Bosch, and W. van de Water, Nature **372**, 48 (1994).
  - [22] M. Cross and P. Hohenberg, Science **263**, 1569 (1994).
  - [23] A. Torcini, A. Politi, G.-P. Puccioni, and G. D'Alessandro, Physica **D 53**, 85 (1991).
  - [24] Y. B. Pesin, Russian Math. Surveys **32**, 55 (1977).
  - [25] S. Lepri, G. Giacomelli, A. Politi, and F. Arecchi, Physica **D 70**, 235 (1993).
  - [26] J. Dormand and P. Prince, Comp. & Maths. Appls. **12A**, 1007 (1986).
  - [27] I. Shimada and T. Nagashima, Prog. Theor. Phys. **61**, 1605 (1979).
  - [28] G. Benettin, L. Galgani, A. Giorgilli, and J.-M. Strelcyn, Meccanica **15**, 21 (1980).
  - [29] T. S. Parker and L. O. Chua, *Practical Numerical Algorithms for Chaotic Systems*, (Springer, New York, 1989).

## APPENDIX: NUMERICAL ALGORITHMS APPLIED

The differential equations were integrated using a Runge-Kutta triple [26]. This algorithm takes advantage of a sixth-order formula to propagate a system of ordinary differential equations. A fifth-order formula is used to estimate the integration error and, additionally, for each Runge-Kutta step  $t_n \rightarrow t_{n+1}$ , the algorithm calculates a polynomial that approximates the solution on the whole interval  $[t_n, t_{n+1}]$  up to an error of fifth order. The tolerance was set to  $10^{-10}$ .

The Poincaré sections were obtained via parabolic interpolation in the vicinity of the intersection points. To calculate the bifurcation diagrams, we utilized a simple algorithm. For each value of  $a$ , we started with the state of the system for the last value of  $a$ , let the system adjust to the changed parameter value for a transient time equivalent to some thousand revolutions, and then recorded the intersection points.

Lyapunov exponents were calculated using the algorithm described in [27–29]. This algorithm tracks the time development of an orthonormal basis in the tangent space of phase space. At regular time intervals ( $\Delta T = 50$  in our

case), the vectors are reorthonormalized. The mean logarithmic growth rates of the moduli of the vectors are the Lyapunov exponents.

The delay equation of the time-delayed control was integrated by the same Runge-Kutta triple, using the spline polynomials that the Runge-Kutta triple outputs to record the continuous history of  $(\mathbf{x}, x_N)$ . The control acts on all variables of the system. We choose a gain factor of 0.05 and limited the control signal to 25% of the modulus of the corresponding time derivative of the uncontrolled GRS. For the delay time  $\tau$ , we choose the eigenfrequency of the oscillator to be stabilized and, subsequently, adjusted  $\tau$  to minimize the mean control signal.

Figure 1. Schematical representation of the structure of the GRS in (a) the Baier-Sahle picture, (b) the mode picture. Each circle represents one linear degree of freedom, the square represents a nonlinear degree of freedom.

Figure 2. The real parts of the eigenvalues of the central fixed point  $(\mathbf{x}^{(1)}, x_N^{(1)})$  close to the Hopf bifurcations that give rise to the coexisting attractors ( $N = 7$ ) plotted as a function of parameter  $a$ .

Figure 3. Bifurcation diagram for  $N = 5$  under variation of  $a$ . Shown is the projection of the Poincaré section onto  $z_2$  (intersection at  $z_1 = 0$ , parameters:  $\varepsilon = 0.1$ ,  $b = 4$ ,  $d = 2$ ).

Figure 4. Lyapunov spectrum for  $N = 5$  under variation of  $a$ . The diagram shows the Lyapunov exponents  $\lambda$  on attractor 1, except for the grey-shaded area, where attractor 1 does not exist (parameters:  $\varepsilon = 0.1$ ,  $b = 4$ ,  $d = 2$ ).

Figure 5. Period-1 orbit for  $N = 5$  on attractor 1; 1:2 mode locking; projections onto (a) oscillator  $(z_1, z_2)$  and  $x_5$ , (b) oscillator  $(z_3, z_4)$  and  $x_5$  (parameters:  $a = 0.04$ ,  $\varepsilon = 0.1$ ,  $b = 4$ ,  $d = 2$ ).

Figure 6. Chaotic orbit for  $N = 5$  on attractor 1. Projections onto (a) oscillator  $(z_1, z_2)$  and  $x_5$ , (b) oscillator  $(z_3, z_4)$  and  $x_5$  (parameters:  $a = 0.085$ ,  $\varepsilon = 0.1$ ,  $b = 4$ ,  $d = 2$ ).

Figure 7. Period-1 orbit for  $N=5$  on attractor 2; 2:1 mode locking. Projections onto (a) oscillator  $(z_1, z_2)$  and  $x_5$ , (b) oscillator  $(z_3, z_4)$  and  $x_5$  (parameters:  $a = 0.04$ ,  $\varepsilon = 0.1$ ,  $b = 4$ ,  $d = 2$ ).

Figure 8. Chaotic orbit for  $N = 5$  on attractor 2; projections onto (a) oscillator  $(z_1, z_2)$  and  $x_5$ , (b) oscillator  $(z_3, z_4)$  and  $x_5$  (parameters:  $a = 0.1$ ,  $\varepsilon = 0.1$ ,  $b = 4$ ,  $d = 2$ ).

Figure 9. The transient onto the period-1 orbit of attractor 2 under the action of the time-delay control: (a) projection onto oscillator  $(z_1, z_2)$  and  $x_5$ , (b) projection onto oscillator  $(z_3, z_4)$  and  $x_5$ , (c) time development of the amplitude  $A$  of the control signal  $|\mathbf{x}(t) - \mathbf{x}(t - \tau)|$  (parameters:  $N = 5$ ,  $a = 0.12$ ,  $\varepsilon = 0.1$ ,  $b = 4$ ,  $d = 2$ ; parameters of the control:  $\tau = 3.8557$ , control gain  $\kappa = 0.05$ , control limit  $= 0.25$ ).

Figure 10. Time development of the mean amplitudes  $r_1 = \sqrt{z_1^2 + z_2^2}$  and  $r_2 = \sqrt{z_3^2 + z_4^2}$  of the two oscillators in the mode picture after the time-delay control has been switched off. The trajectory remains in the basin of attraction of attractor 1 until  $t \simeq 9500$ . At this point, it quickly moves into the basin of attraction of attractor 2 and never returns to attractor 1 afterwards (parameters:  $N = 5$ ,  $a = 0.12$ ,  $\varepsilon = 0.1$ ,  $b = 4$ ,  $d = 2$ ).

Figure 11. Hyperchaotic orbit for  $N = 5$ ; projections onto (a) oscillator  $(z_1, z_2)$  and  $x_5$ , (b) oscillator  $(z_3, z_4)$  and  $x_5$  (parameters:  $a = 0.3$ ,  $\varepsilon = 0.1$ ,  $b = 4$ ,  $d = 2$ ).

Figure 12. Bifurcation diagram for  $N = 7$ : attractor 1, attractor 2, and attractor 3 from bottom to top in different shadings. The values of  $x_6$  at the maxima of  $x_6$  are shown (parameters:  $\varepsilon = 0.1$ ,  $b = 4$ ,  $d = 2$ ).

Figure 13. Lyapunov spectrum for  $N = 7$ : depicted is up to  $a = 0.06$  the development on attractor 1, from  $a = 0.06$  to  $a = 0.11$  that on attractor 2 (grey-shaded), above  $a = 0.11$  that on the remaining large attractor.

Figure 14. (a)-(c): Periodic orbit for  $N = 7$ ,  $a = 0.035$  on attractor 2 with 1:1:1 mode locking: projections onto (a) oscillator  $(z_1, z_2)$  and  $x_7$ , (b) oscillator  $(z_3, z_4)$  and  $x_7$ , (c) oscillator  $(z_5, z_6)$  and  $x_7$ . (d)-(f): Chaotic orbit for  $N = 7$ ,  $a = 0.095$  on attractor 2; projections onto (d) oscillator  $(z_1, z_2)$  and  $x_7$ , (e) oscillator  $(z_3, z_4)$  and  $x_7$ , (f) oscillator  $(z_5, z_6)$  and  $x_7$  (other parameters:  $\varepsilon = 0.1$ ,  $b = 4$ ,  $d = 2$ ).

Figure 15. Time development of the GRS for  $N = 61$ . The amplitudes of the variables  $x_{2n-1}$  are shown in grey scale as a function of time for (a)  $a = 0.03$ , (b)  $a = 0.07$ , (c)  $a = 0.15$  (other parameters:  $\varepsilon = 0.1$ ,  $b = 4$ ,  $d = 2$ ).

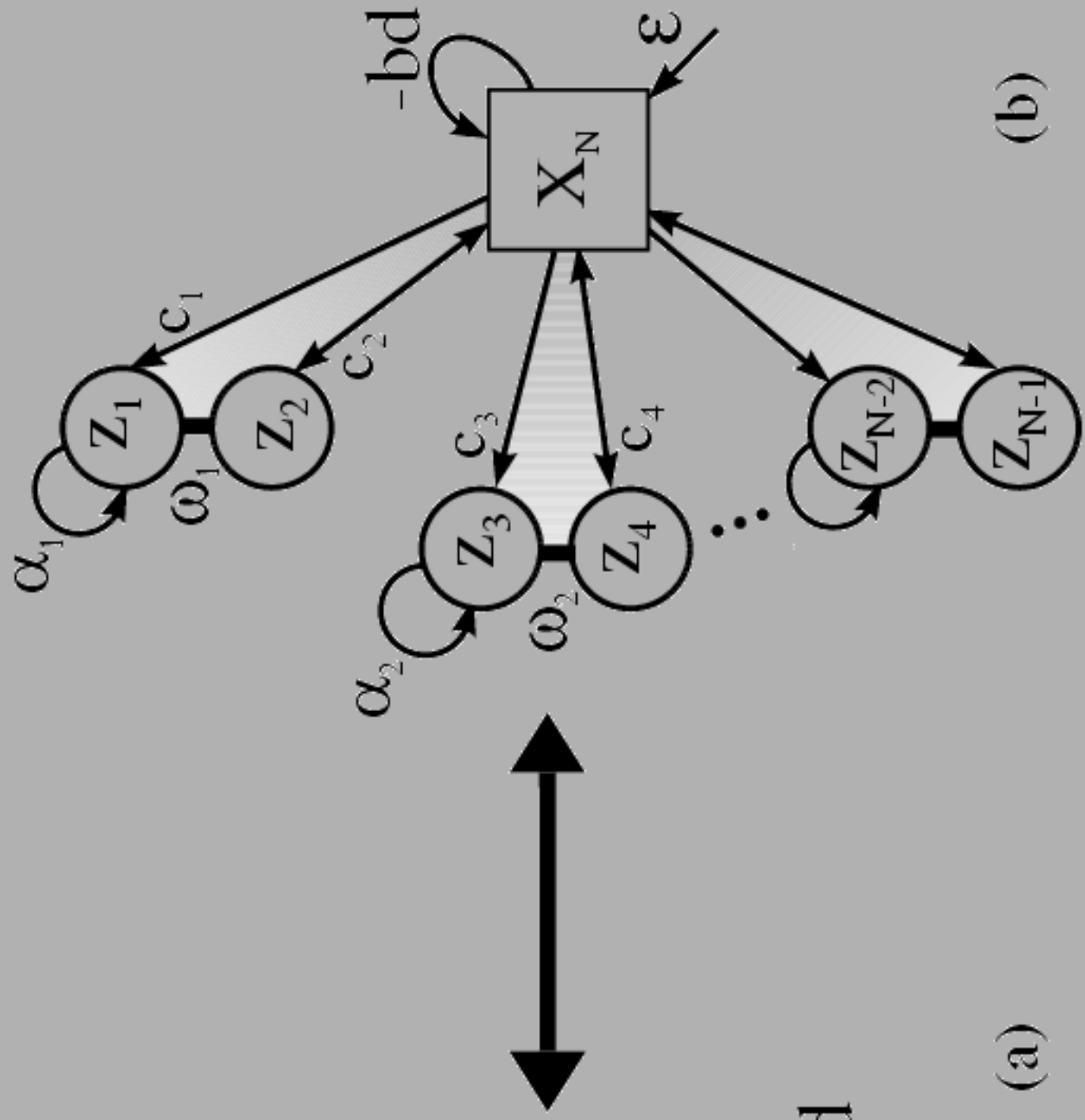
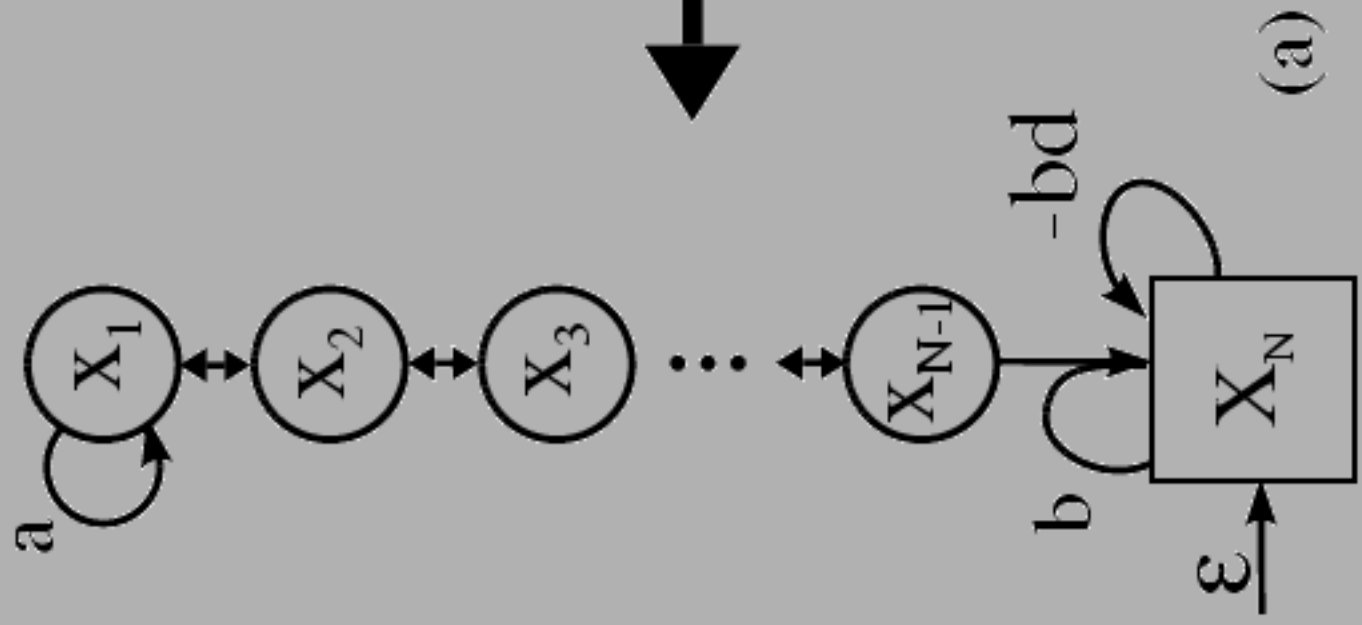
Figure 16. (a) Number of positive Lyapunov exponents, (b) Lyapunov dimension, and (c) metric entropy as a function of  $N$  for  $a = 0.3$ ,  $a = 0.25$ ,  $a = 0.15$ ,  $a = 0.07$  (other parameters:  $\varepsilon = 0.1$ ,  $b = 4$ ,  $d = 2$ )).

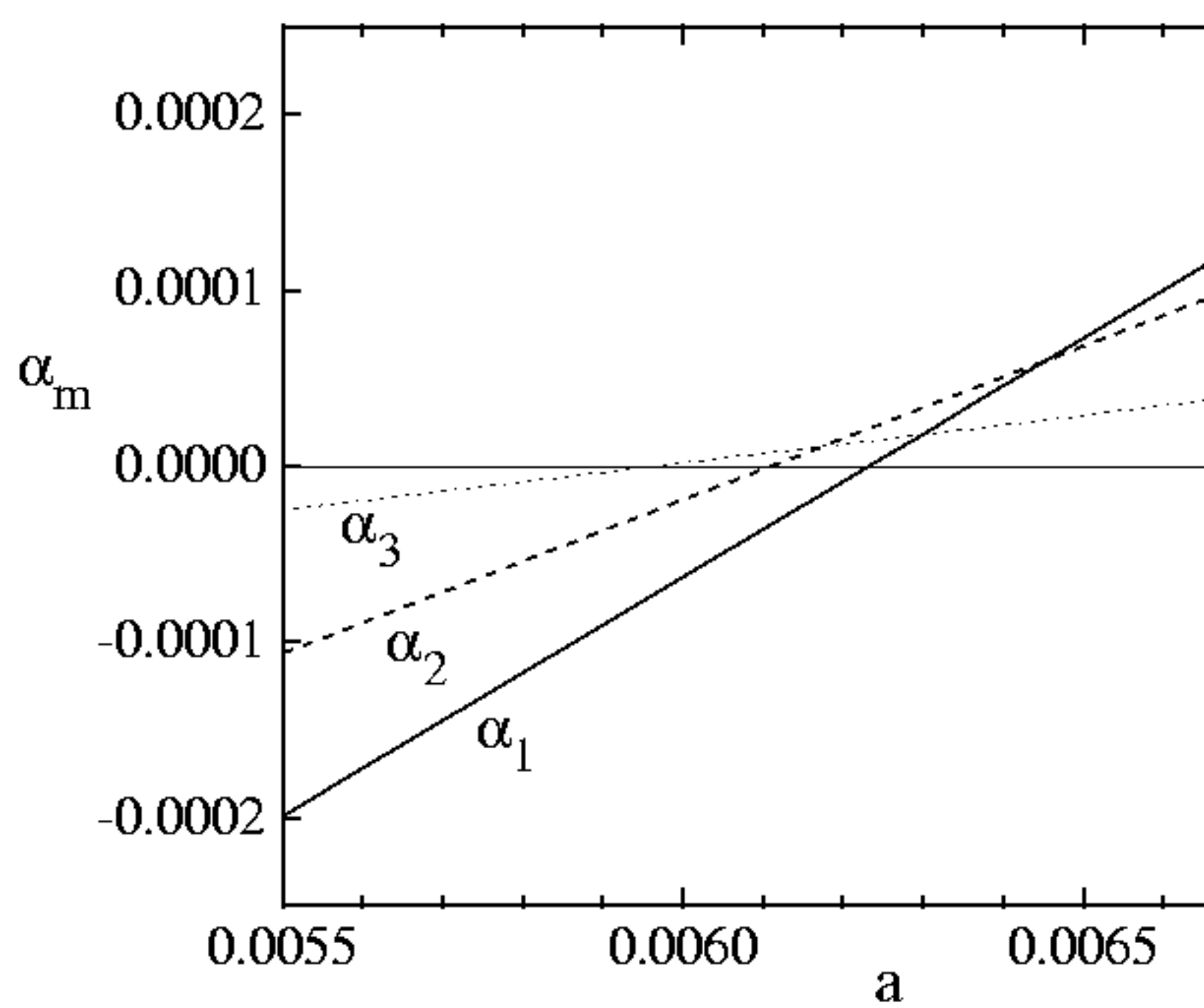
Figure 17. Distribution of rescaled Lyapunov exponents  $\lambda_s = \frac{N^+}{\sum_{\lambda^+}} \lambda$  for different  $N$  ( $N = 15, 21, 41, 61$ ). The Lyapunov exponents are sorted in descending order (parameters:  $a = 0.3$ ,  $\varepsilon = 0.1$ ,  $b = 4$ ,  $d = 2$ )).

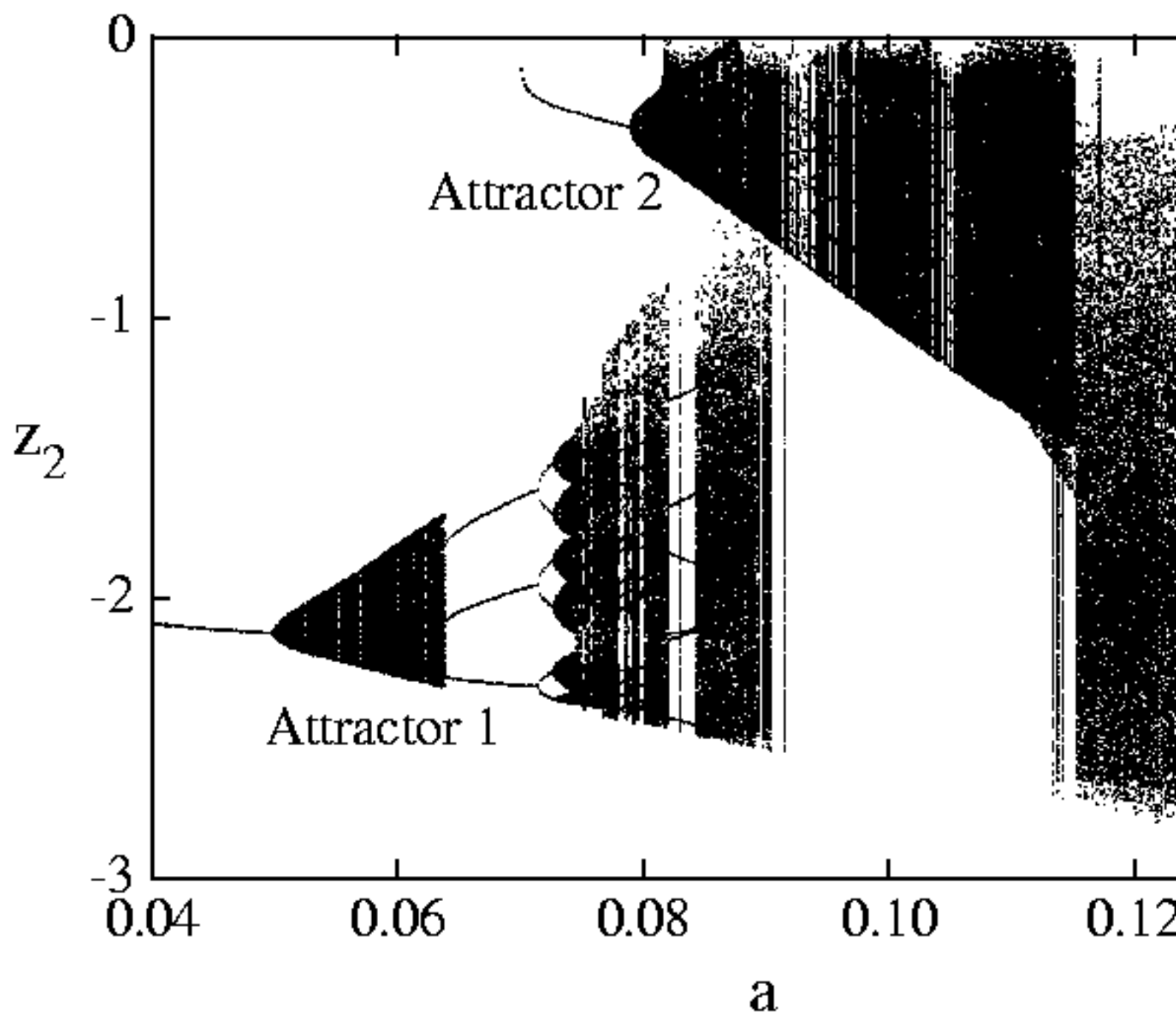
Figure 18. Comparison of the real parts of the eigenvalues of the linear subsystem  $\alpha_i$  and the Lyapunov exponents of the GRS in the case  $N = 61$  for  $a = 0.07$ ,  $a = 0.15$ , and  $a = 0.25$ . Here, all values have been divided by the respective values of  $a$ , in order to get comparable values for different  $a$ . (other parameters:  $\varepsilon = 0.1$ ,  $b = 4$ ,  $d = 2$ ).

| a    | $H_\infty$ | $\frac{H_\infty}{a}$ |
|------|------------|----------------------|
| 0.3  | 0.2        | 0.7                  |
| 0.25 | 0.16       | 0.6                  |
| 0.15 | 0.08       | 0.5                  |
| 0.07 | 0.02       | 0.3                  |
| 0.03 | 0.0        | 0.0                  |

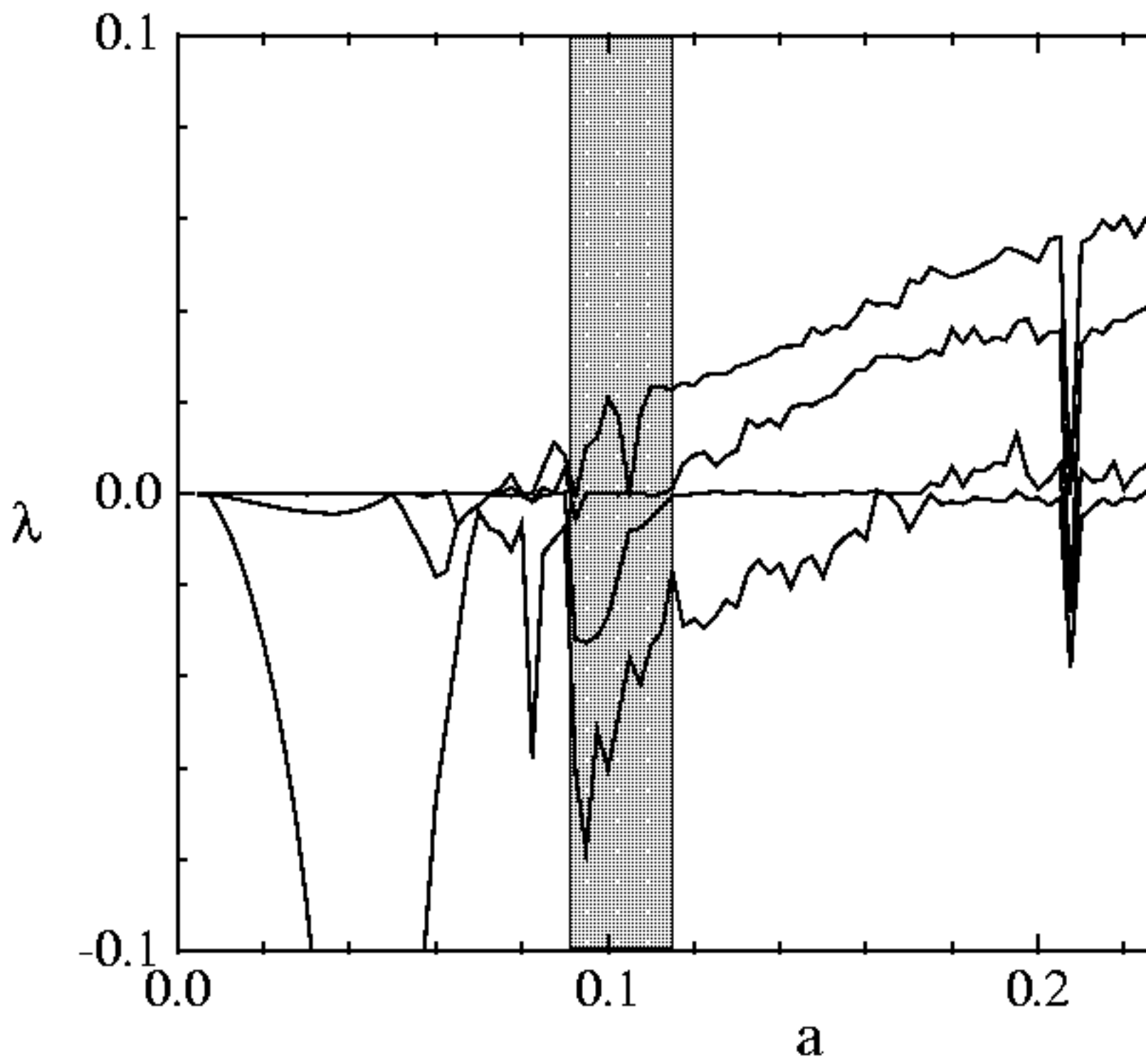
Table I. Limit value of the metric entropy  $H$  for different values of  $a$ .

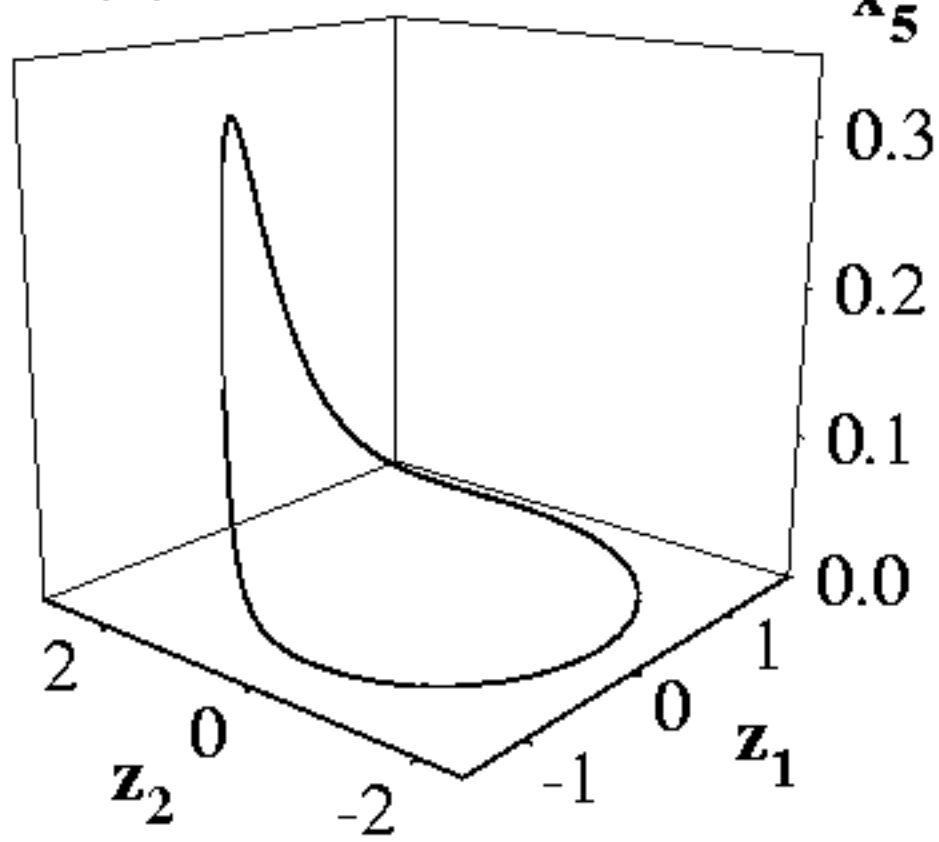
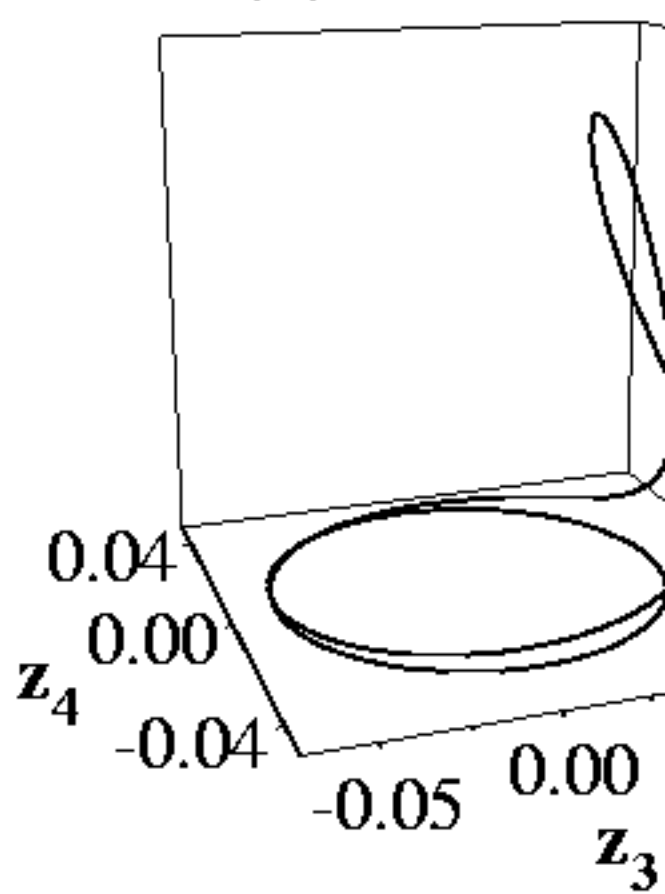


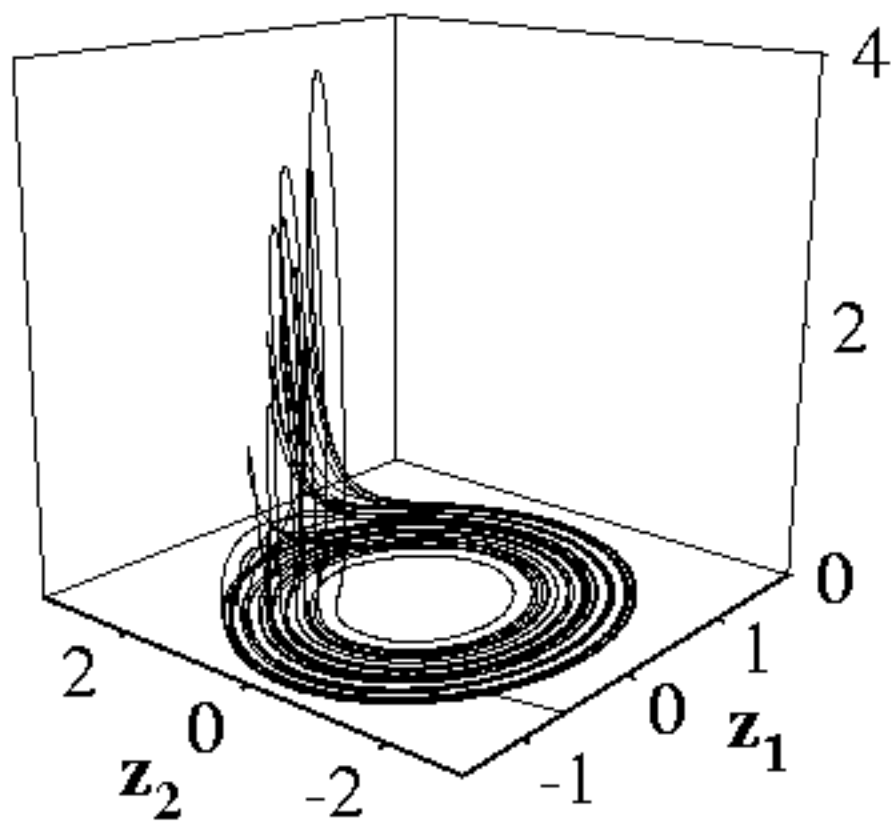
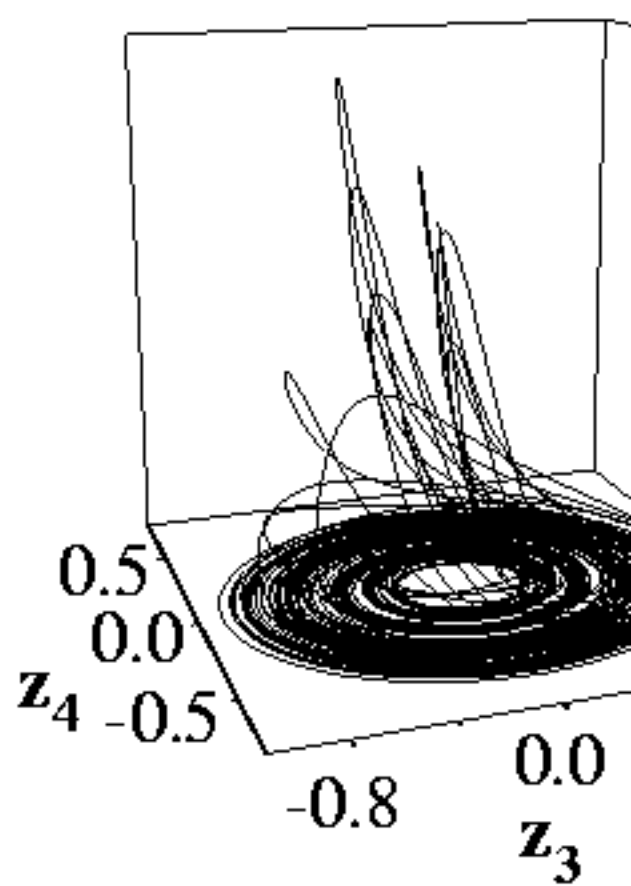


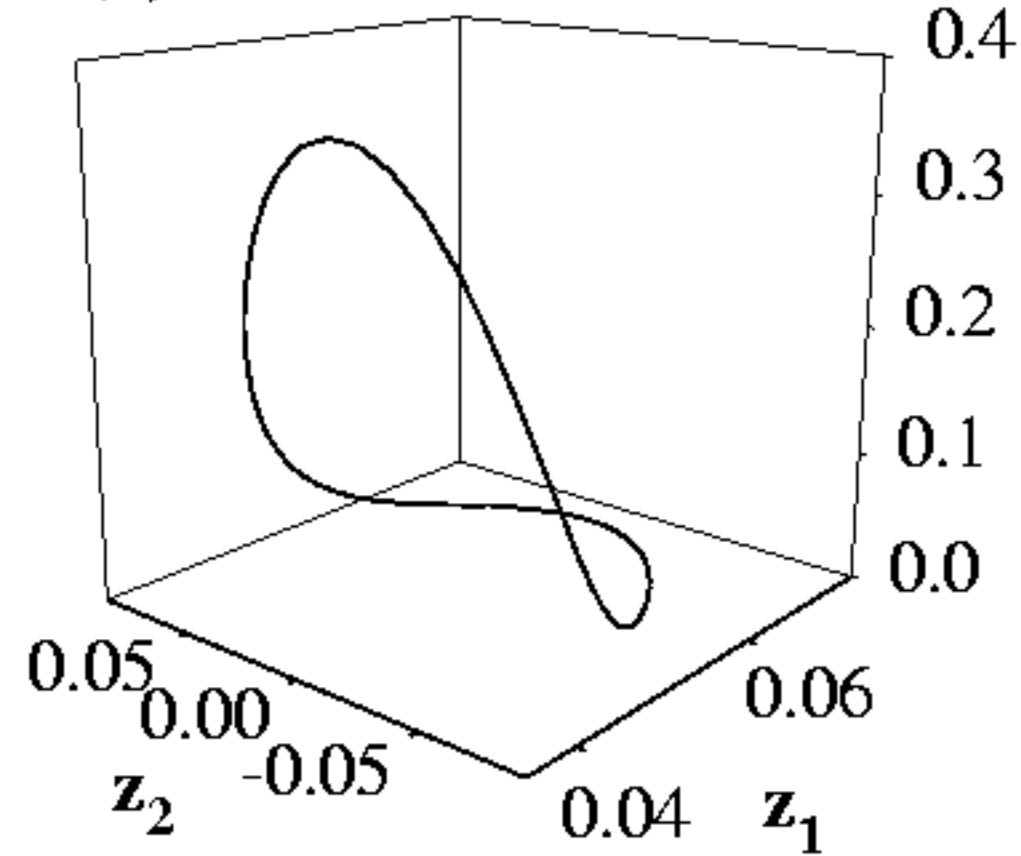
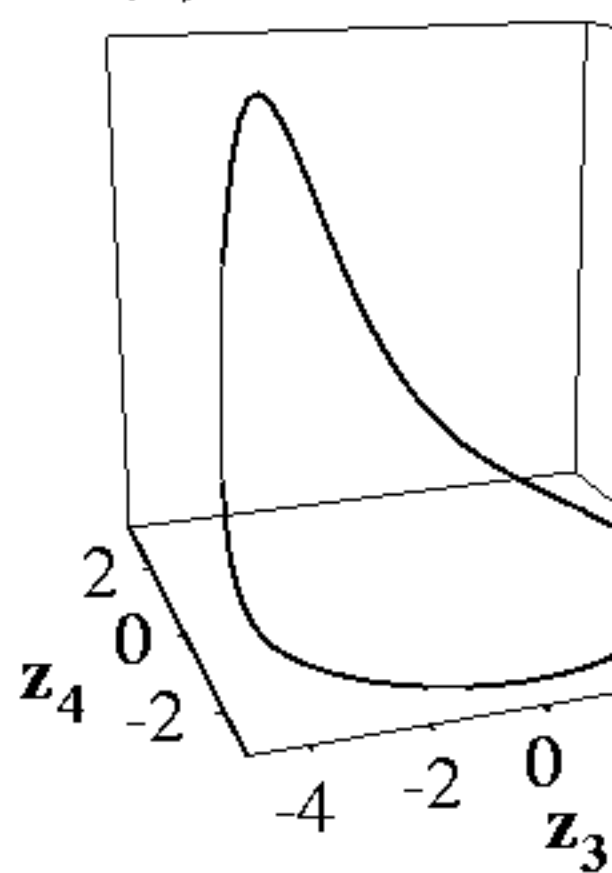


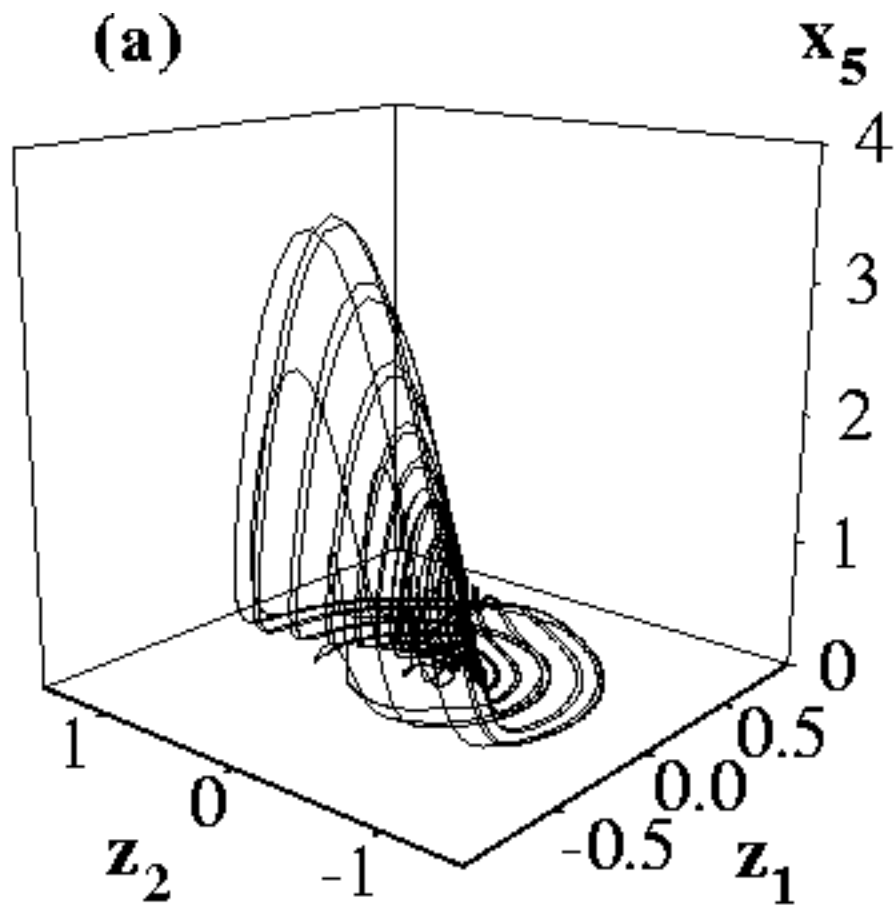
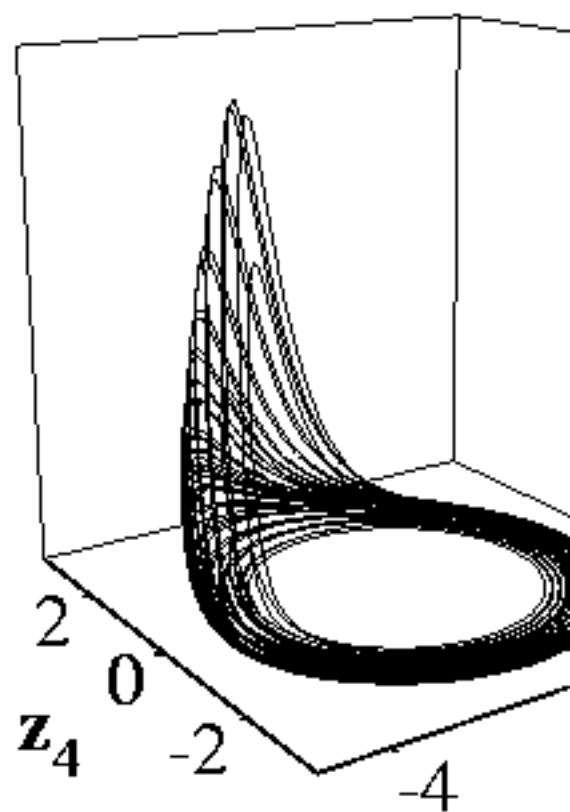


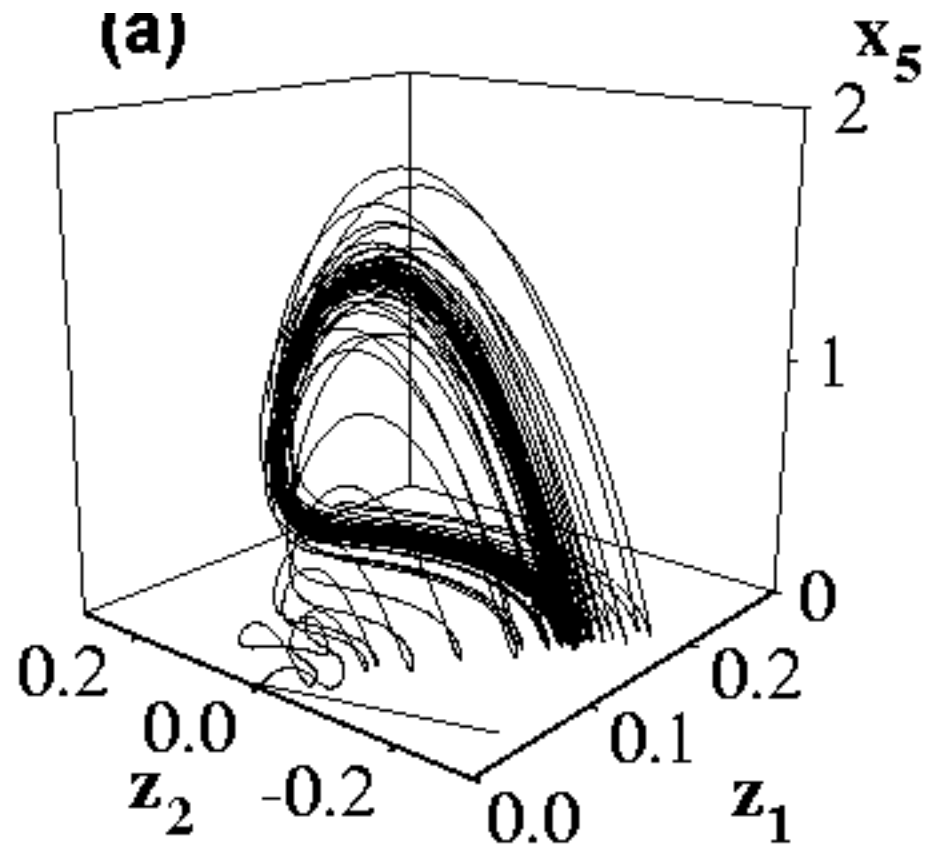
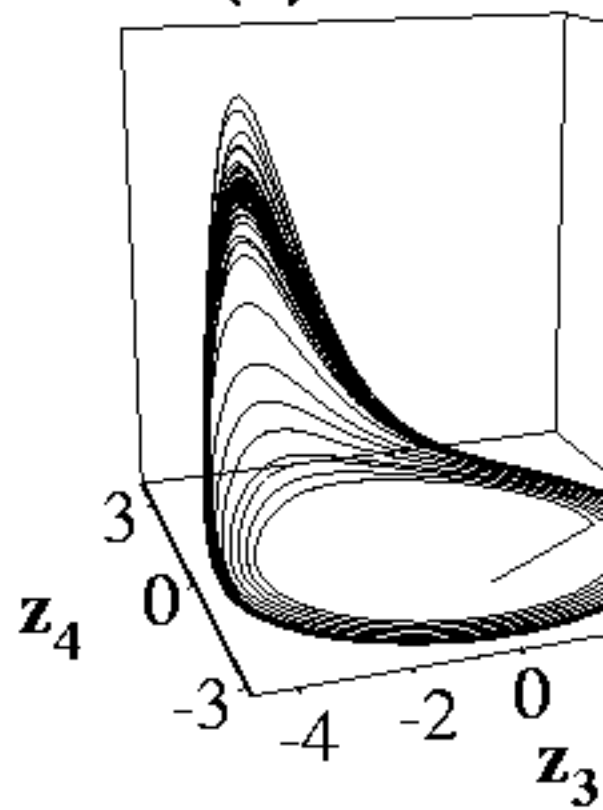


**(a)****(b)**

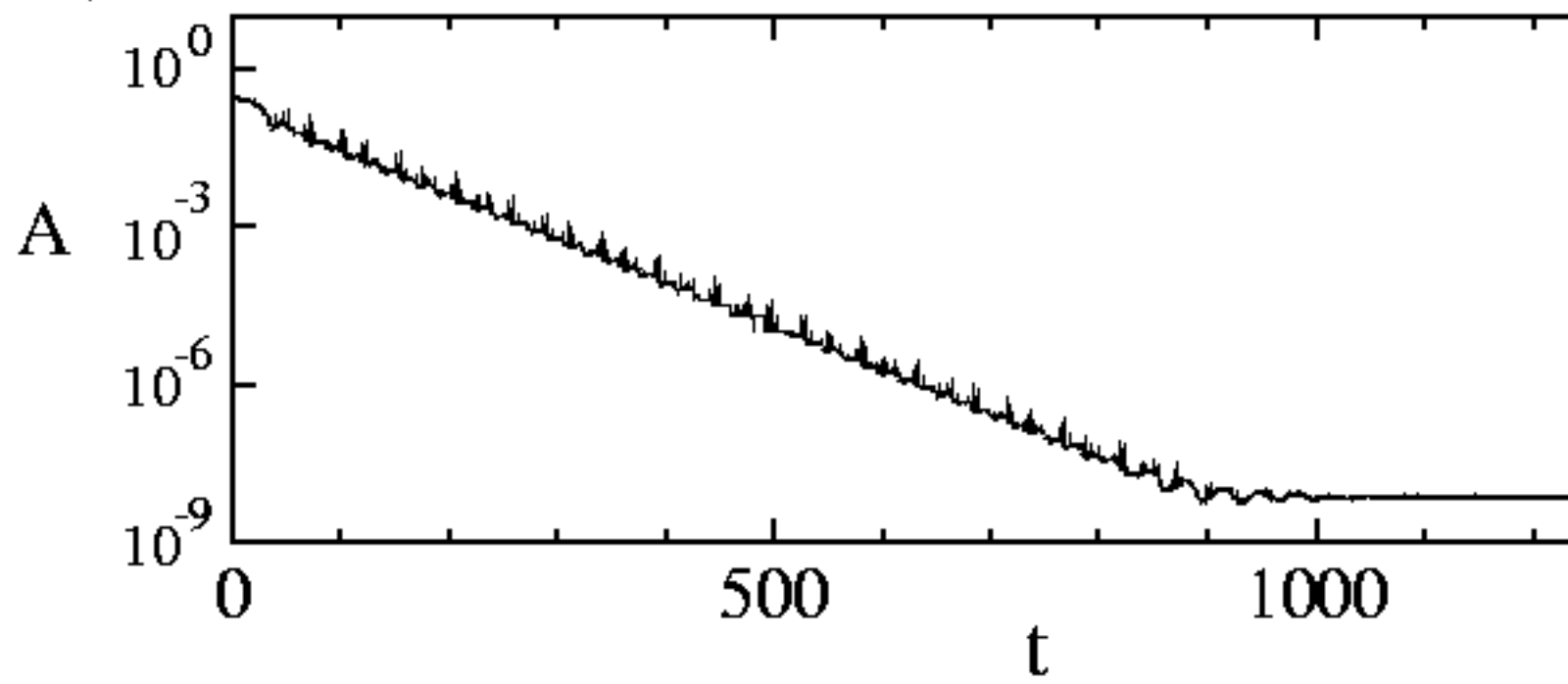
**(a)****(b)**

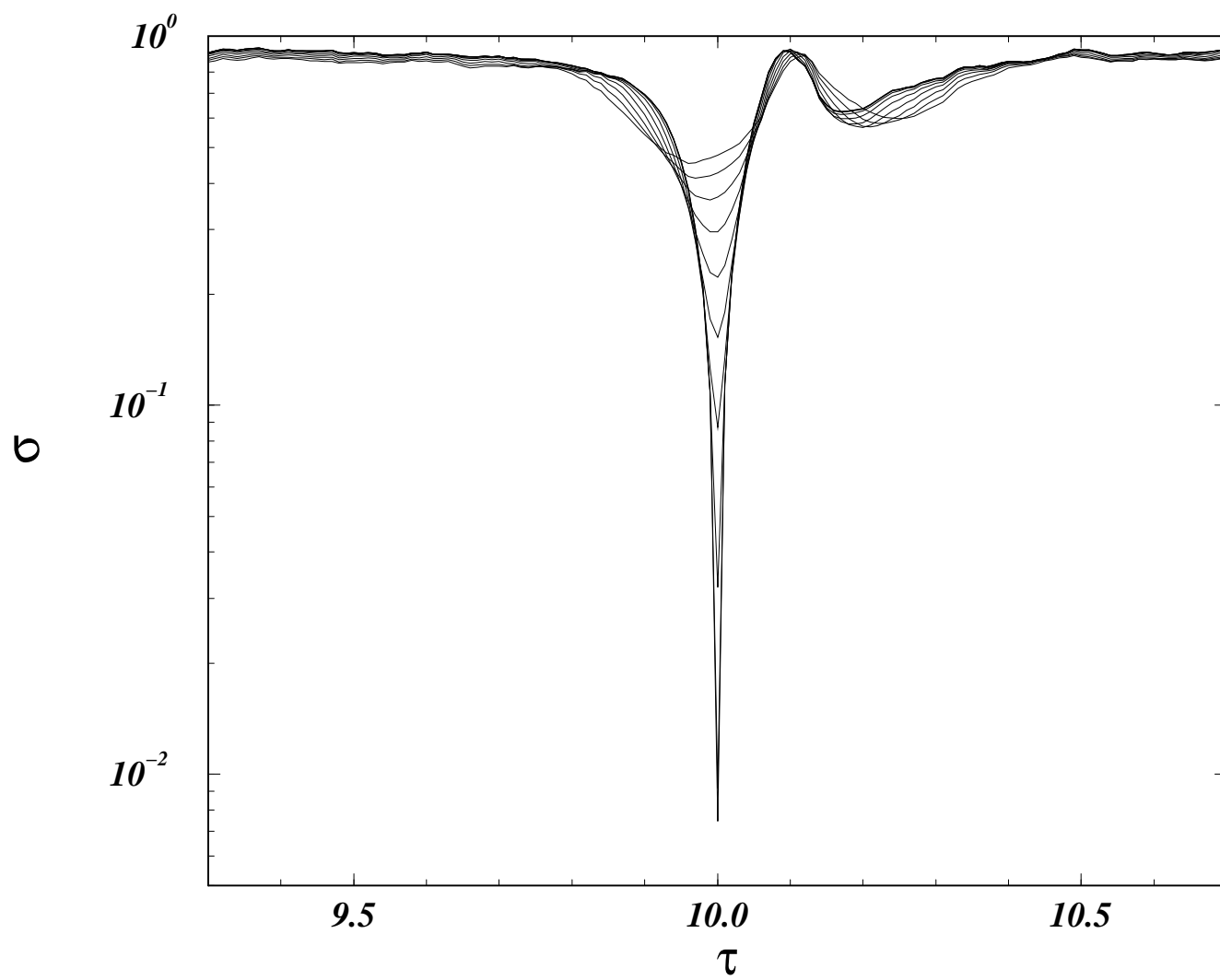
**(a)****(b)**

**(a)****(b)**

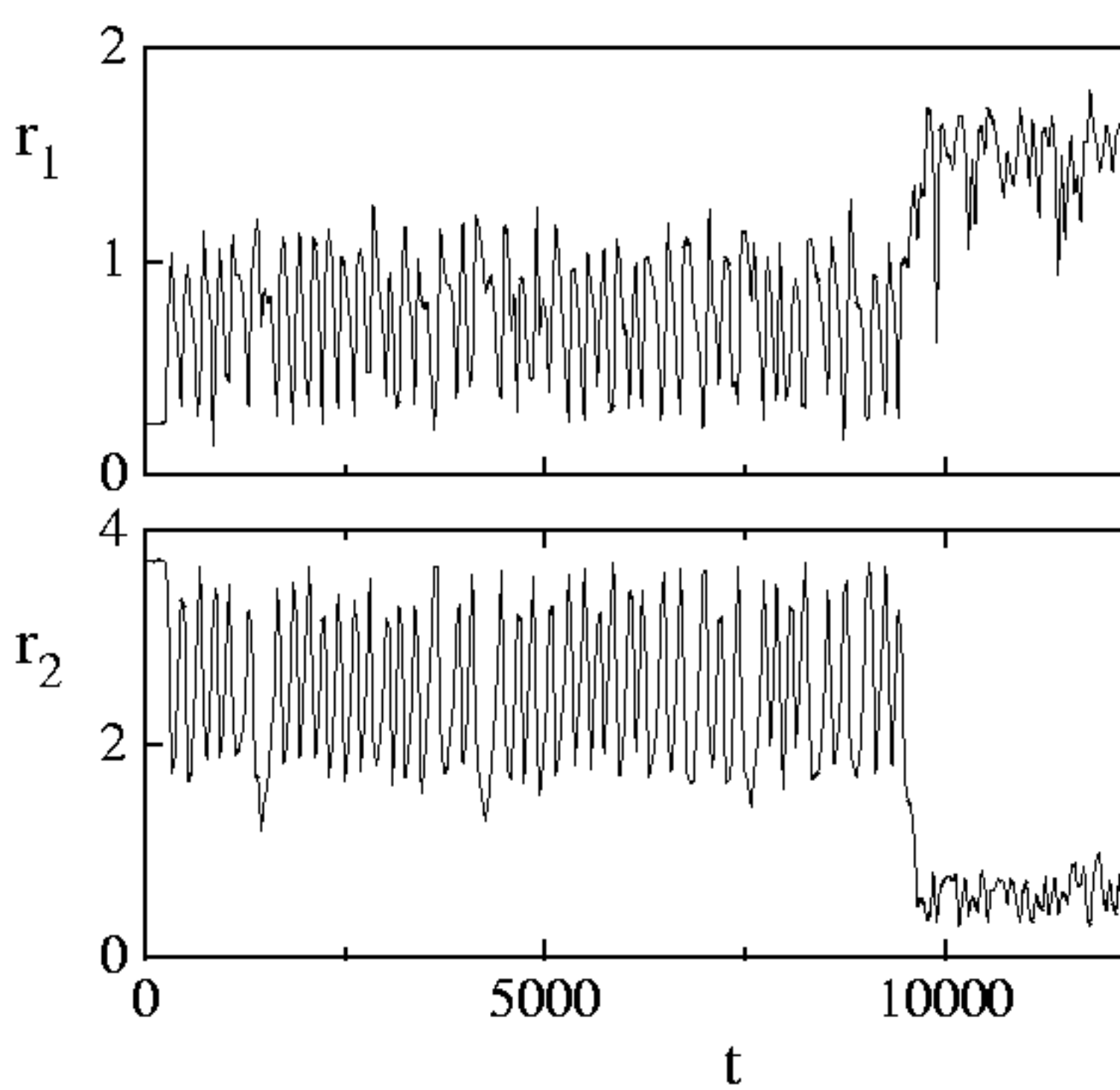
**(a)****(b)**

(c)

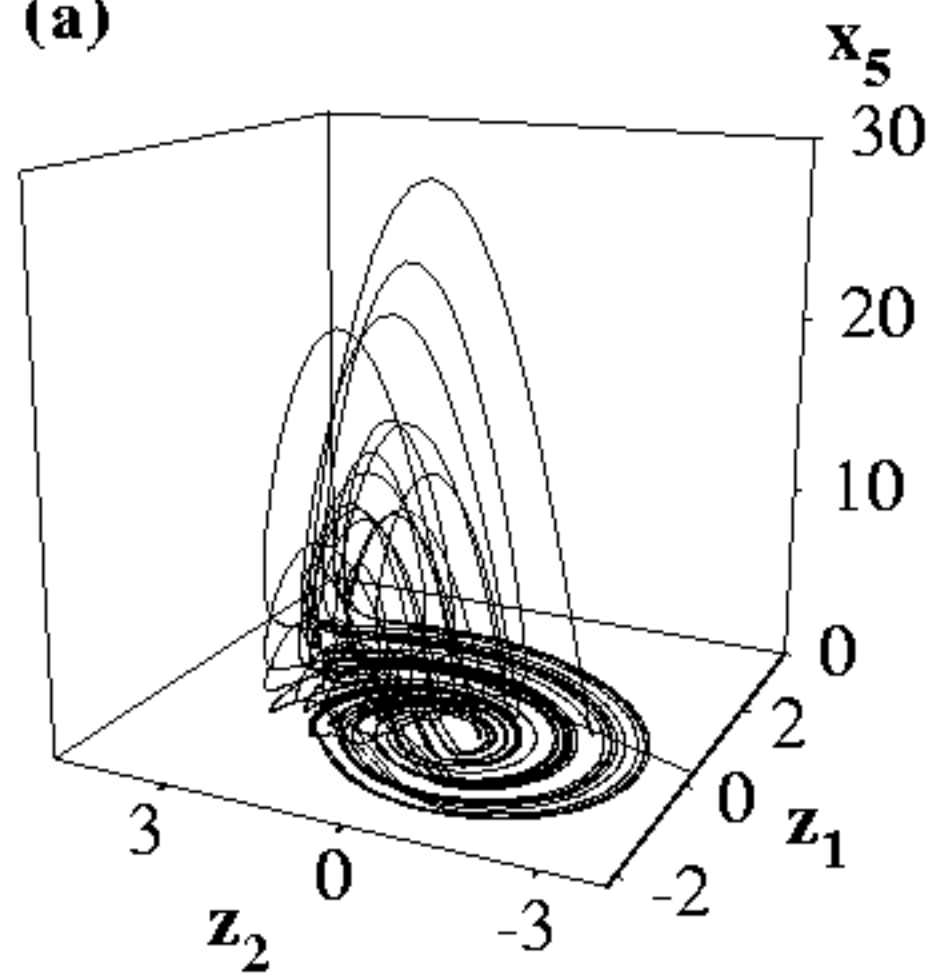




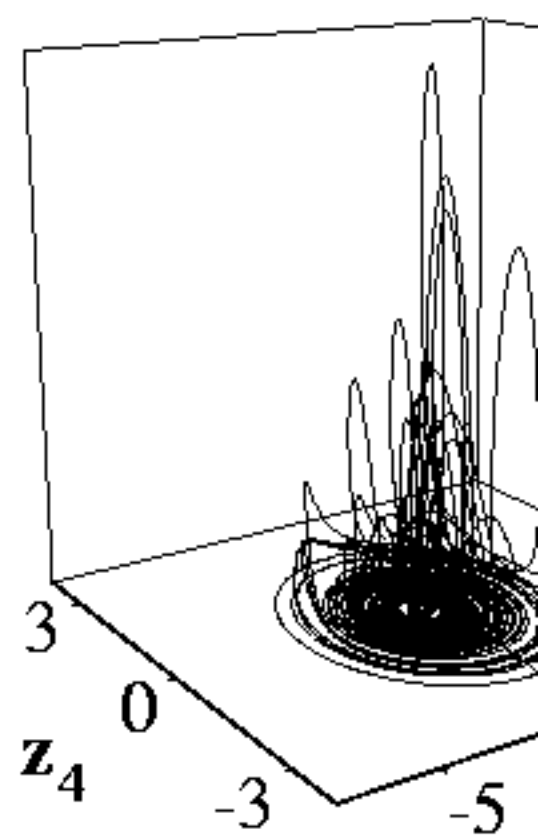


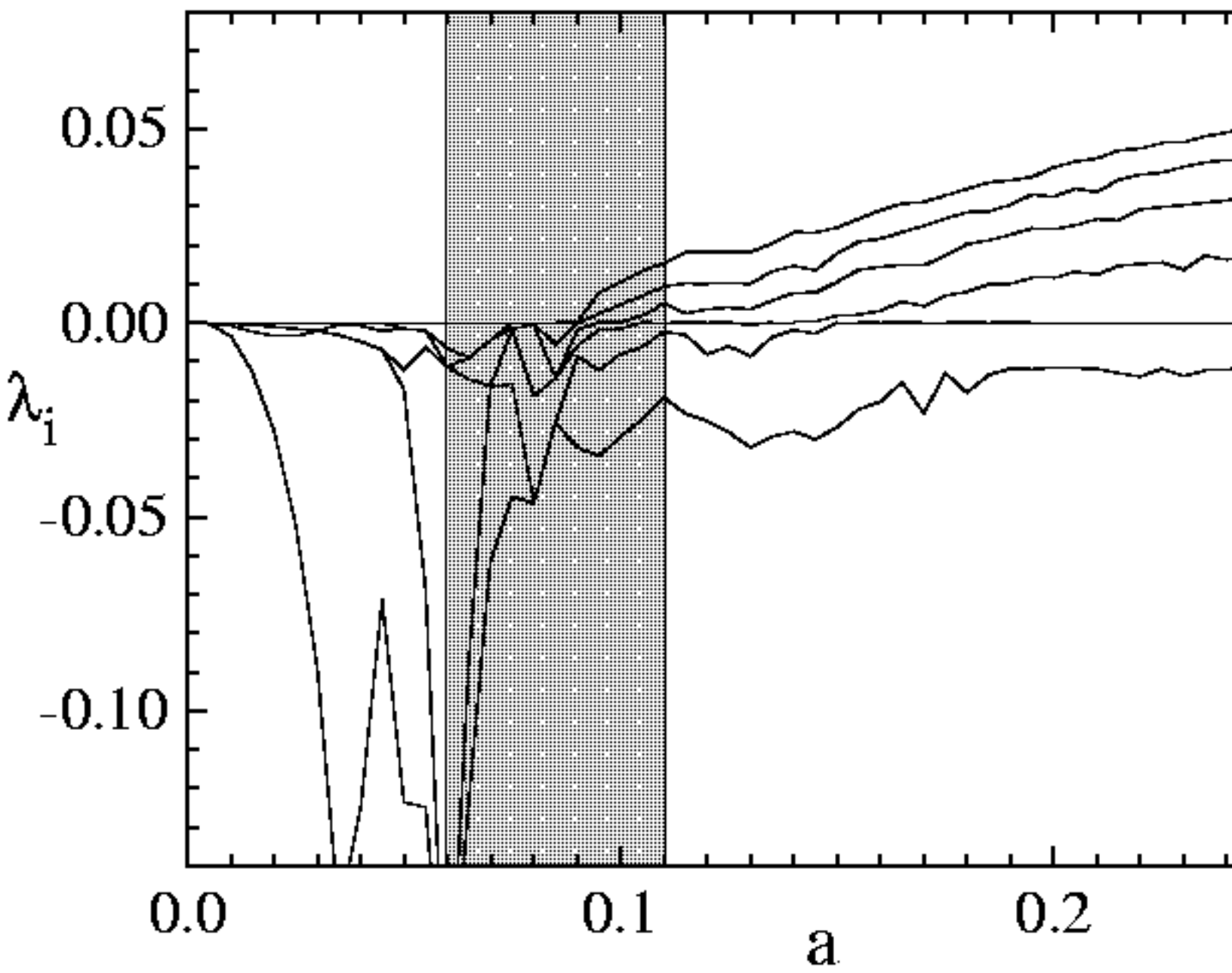


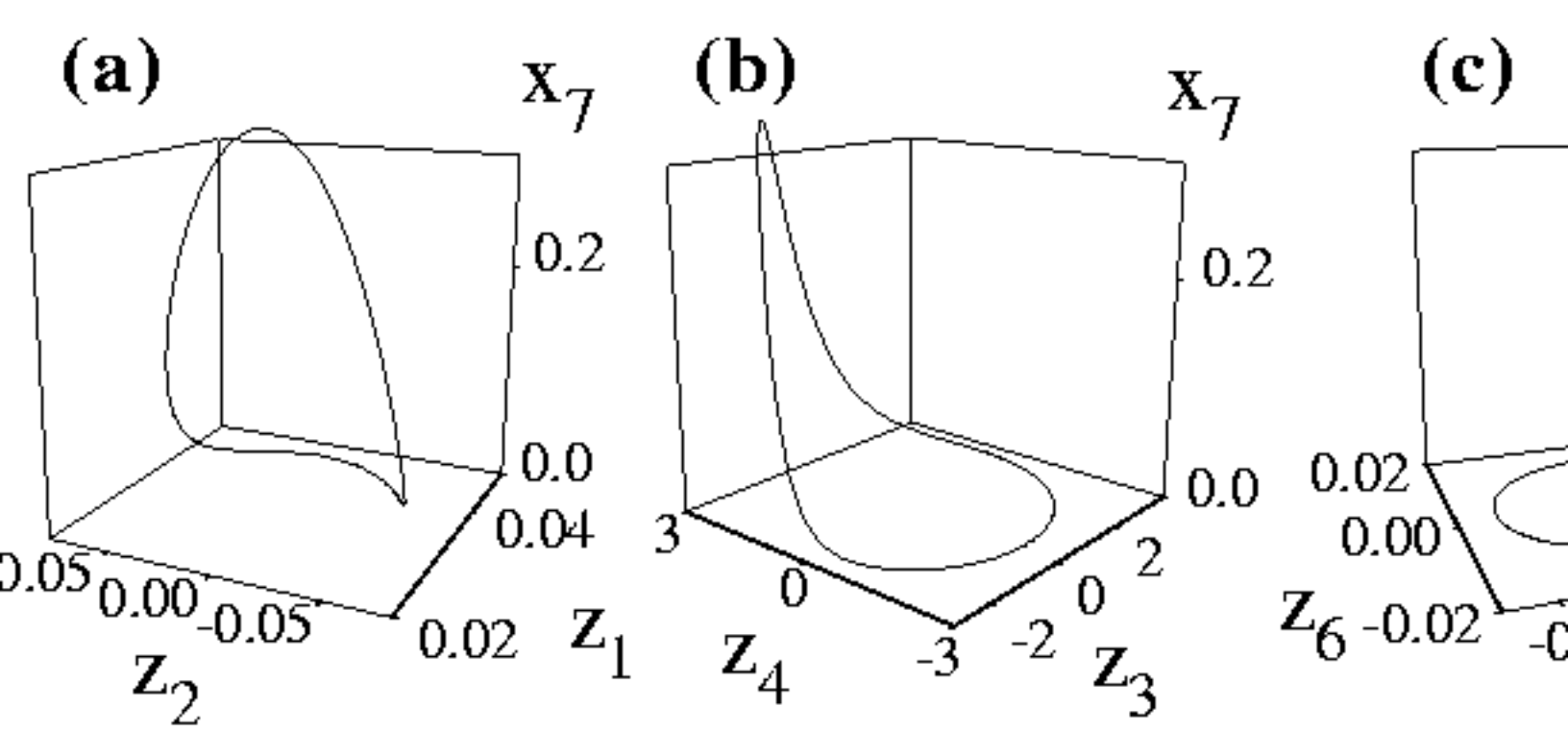
**(a)**

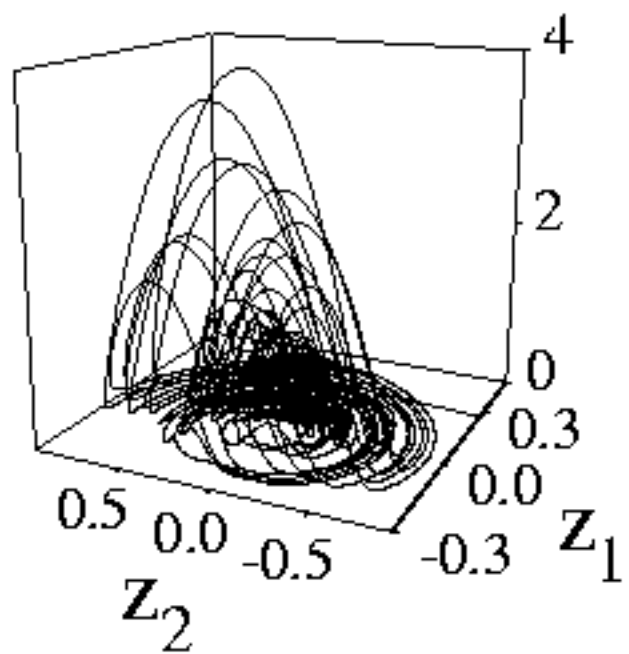
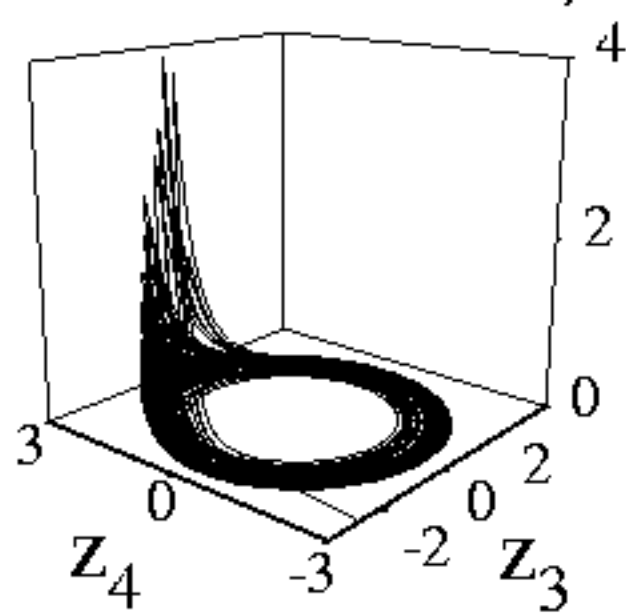


**(b)**







**(d)** $x_7$ **(e)** $x_7$ **(f)**